COMPREHENSIVE GAS RESERVOIR AND WELLBORE COUPLED MODEL TO STUDY LIQUID LOADING

A Dissertation

by

MOHAMMAD F KH O KH ALDOUSARI

Submitted to the Office of Graduate and Professional Studies of
Texas A&M University
in partial fulfillment of the requirements for the degree of

DOCTOR OF PHILOSOPHY

Chair of Committee,	A. Rashid Hasan
Co-Chair of Committee,	Ding Zhu
Committee Members,	Jenn-Tai Liang
	Yuefeng Sun
Head of Department,	Jeff Spath

May 2019

Major Subject: Petroleum Engineering

ABSTRACT

Simulating gas flow from the reservoir to the wellhead is a complicated task often done by a commercial software or overlay simplified coupled model based on one inflow equation. The commercial software requires specialized training as they are cumbersome and time-consuming. Besides, they cannot be modified to accommodate any research idea requiring additional or different approaches. In this study, a simple, comprehensive reservoir-wellbore coupled model is presented to be used by researchers or engineers in the field where the access to fully fledged simulation is unavailable.

The proposed model consists of two systems. The wellbore system depends on a two-phase mechanistic model to calculate all fluid properties and pressure drop along the wellbore. The reservoir system relies on Darcy flow equations and relative permeability correlations to estimate the inflow flow rate for each phase. Finally, gas reservoir material balance is used to obtain reservoir pressure for every time step. This model is implicit and dynamic.

After validating the model with field data and commercial software, several case studies were created to investigate gas well related issues. The proposed models can investigate the liquid loading phenomena where the gas is unable to lift the liquid droplets to the surface. The model can predicate the onset of the liquid loading and the time needed for liquid to kill the well by examining wellbore fluid changes throughout the wellbore. The transition of flow pattern from annular to churn flow is considered the initiation of this phenomena. The model can present a visual picture of flow pattern changes through the well's life.

Using the proposed model as a diagnostic tool, Hasan-Kabir model has been modified by introducing smoothing flow pattern transition equations.

ACKNOWLEDGEMENTS

I would like to thank my committee chair, Dr. Hasan, and my committee members, Dr. Zhu, Dr. Liang, and Dr. Sun.

CONTRIBUTORS AND FUNDING SOURCES

This work was supervised by a dissertation committee consisting of Professor A. Rashid Hasan and Professors Ding Zhu and Jenn-Tai-Liang of the Department of Petroleum Engineering and Professor Yuefend Sun of the Department of Geology & Geophysics. All work for the dissertation was completed independently by the student.

Graduate study was supported by a sponsorship from Kuwait University.

TABLE OF CONTENTS

Page

LIST OF FIGURES

Page

LIST OF TABLES

Page

CHAPTER I

INTRODUCTION AND LITERATURE REVIEW

Introduction

This work is a comprehensive study on two-phase flow in the wellbore. The flowing of different phases simultaneously presents a significant challenge to researchers. Both phases have different properties and behave differently under the same pressure and temperature. One phase is denser than the other phase. One phase flows faster than the other. These differences demand a deep understanding of the two-phase flow inside the tubing.

The topic of two-phase flow in pipelines has been exhausted with studies over the years. This issue is not exclusive only in the petroleum industry. Other branches of engineering, like mechanical, chemical, and even nuclear are investigating this topic. In petroleum production engineering, the attention went exclusively and for a long time to the wellbore itself and the flow inside the wellbore as petroleum engineering is a new field of study relatively, and the founders of it, are chemical and mechanical engineers.

Tulsa University petroleum engineering department has invested in establishing a full production loop. They have been studying flow assurance for quite some time. One of the leading research area investigated by them is the two-phase flow in pipelines. They studied the early concept presented by Turner et al. (1967) extensively by observing fluid flow inside wellbores with a high-speed camera capturing the flow to the fraction of the seconds. How gas and liquid flow? The shape of their flow? The effect of each phase on the other? All these questions were answered. Also, they have developed several correlations mechanistic and empirical to predict pressure loss in pipelines. The door to improve these correlation or models

welcomed has welcomed many researchers over the years. Researchers are trying to improve a little bit over the previous work. The accuracy of predicting pressure drop in pipelines.

The question might arise, why there is a need to predicate the pressure drop inside the wellbore? Predicting pressure drop can aid in understanding the declining flow rate. All the petroleum companies wish for more production. Production meets their expectation which is based on similar wells in the same area. To know the reason of decline production is to run a pressure drop study. Comparing the finding of the study to the actual pressure drop can either result in agreement with the actual decline and that this is the normal behavior of the well, or it does not agree. In this case, the company knows there is something needs further investigation in the wellbore.

In the past 30 years, a great effort invested in improving the prediction of two-phase flow in the wellbore. However, in the recent years, the production engineering researchers became more interested in the reservoir as well. The production as a process consisting of two systems, wellbore system, and reservoir system.

The idea of coupled wellbore-reservoir model became the hot topic. In this study, we present such a model. Coupled model. In the recent previous years, a few good coupled models have been presented in the literature. We have mentioned them in detail in the following section. The idea behind this research is to build a coupled model that is:

1- Robust. A model built upon scientific and engineering sound principles.

2- Realistic. A model gives reliable output represent actual results.

3- Simple. A model can be programmed by anyone who has access to any programming software.

Building this tool/model required extensive research on inflow relationship from the reservoir and two-phase flow in the reservoir. Two-phase-flow in the wellbore is an already established area of research. We have used Hasan-Kabir two-phase mechanistic model, and heat transfer model in the wellbore. In the reservoir system, Darcy flow for both phases is adopted as inflow coming from the reservoir. The main problem we faced is the relative permeability for each phase. How to determine it? With the aid of power laws of permeability, we were able to proceed with Darcy law. However, using relative permeability equation presented another challenge, reservoir water saturation as reservoir pressure depletes is needed. We were able to overcome these challenges by building an implicit dynamic loop consists of three components each component is providing the other one with the data needed to proceed. The three components are:

1- Wellbore pressure and heat, mechanistic model

2- Darcy inflow equation, relative permeability equations

3- Material balance equation and the volumetric in place volume of hydrocarbon

The result is a dynamic model calculating flowrates at the surface, bottomhole pressure, reservoir pressure, and reservoir water saturation at the same time for specific time steps given by the user of the model.

The dissertation, after the introduction and the literature review in this chapter, presents the methodology in the second chapter. A flow chart is provided for easy to follow programming guidelines. In chapter three, three different validations are presented to show the validity of the proposed model, validation against two commercial software, validation against field data, and lastly validation against open source reservoir simulation.

Our primary goal is to study the liquid loading phenomena. However, in the process of doing so, we have created a tool able to study the two-phase flow in the wellbore. After proving the validity of this tool in chapter three, chapter four presents a particular case, where we used the proposed model to study something else, Hasan-Kabir two-phase flow mechanistic model. The proposed model gives a dynamic output. As a result, we can test the implemented models to their fullest and find any shortcoming associated with them to prove the versatility of the proposed model. It opens the door for future work to examine different models.

In chapter five, the focus is on the reservoir pressure as the primary objective of the whole coupled wellbore-reservoir models to study the effect of the reservoir on the wellbore. We examine the reservoir pressure effect on liquid loading and pressure drop inside the wellbore.

Finally, the last chapter presents different aspects of the coupled wellbore-reservoir such as the behavior of liquid holdup in the wellbore with depth. The effect of water production on liquid holding also is examined. In this chapter, the summary of the whole research is given in the conclusion section.

Literature Review

The liquid loading phenomena are the inability of the gas well to lift the coproduced liquid to the surface. The source of liquid is either from the original liquid in the reservoir or condensed liquid as pressure declines. The reservoir pressure depletion is the primary cause of the declining gas flow rate. When reservoir pressure is high, gas velocity is very high and able to lift all liquid droplets and the liquid film coating the well-tubing upward. The liquid is denser than gas, as a result when gas velocity decline to a specific value, gas stream cannot lift the largest droplet upward. This conclusion came initially from Turner et al. (1969). He studied the onset of liquid loading. He found out that the onset occurs when the gas velocity declines to a value below which, the gas flow cannot lift the largest liquid droplet to the surface. This velocity is known as the critical gas velocity or simply Turner et al. (1969) equation.

$$v_{gc} = 3.1\left(0.0022048\ g\sigma_w \frac{\rho_l - \rho_g}{\rho_g^2} \right)^{0.25} \quad 1$$

This equation is a function of both gas and liquid densities, and interfacial tension. This equation has been modified by Belfroid et al. (2008) to account for the well-inclination angle. Barnea (1986) challenged Turner et al. (1969) theory. In his work, he found out that the liquid loading onset starts earlier than the falling of the largest droplet to the surface. He concluded that liquid film coating well tubing breaks first. Following his discovery, he proposed a series of equations studying the film thickness.

The falling liquids cause an increase in the bottomhole pressure. This back pressure decreases reservoir drawdown (the difference between reservoir pressure and bottomhole pressure) this automatically chocks the gas flow rate coming from the reservoir.

In the Inflow Performance Relationship (IPR), the gas flow rate is proportionally related to squared drawdown; as a result, the gas flow rate decreases significantly.

$$q_g = \frac{\left(p^2 - p_{wf}{}^2\right)k_g h}{1{,}424\,\mu_g z(T+460)\ln(0.472\,r_e/r_w)} \qquad 2$$

Liquid loading phenomena reduce the well-life expectancy and ultimately kills gas well losing enormous investment. The best remedy for liquid loading in the gas well is the prevention of its occurring by having some facility on the ground ready to intervene. Predicting liquid loading onset is essential to the petroleum industry. Production engineers invested a lot of time and effort trying to determine the onset of liquid loading.

Initially, Turner et al. (1969) introduced the clerical gas velocity term, as a parameter should be checked at the top of the wellhead to determine the onset of liquid loading. However, in a recent paper published by Riza et al. (2015), he found that the onset of liquid loading should be investigated throughout the entire wellbore. In their approach, they created a reservoir-wellbore coupled model. Their model is simple. They used single pseudosteady state gas inflow equation based on circle reservoir. In the wellbore, they utilized Hasan-Kabir mechanistic two-phase flow pressure drop model and heat transfer model. Their approach is a forward step in studying liquid loading as a big picture by combining the reservoir and the wellbore. However, it is oversimplified. They assumed bottomhole pressure and assumed this pressure to be constant for a fixed period. Then they manually decreased the bottomhole pressure. In other words, they used a constant steady decline factor. As for water flow rate, they used a fixed gas-liquid ratio to handle it. For reservoir pressure, they assumed a constant pressure over a period, and manually imposed an assumed decline rate. They concluded that liquid onset occurs first at the bottom of the gas well. However, their approach has several assumptions that do not represent what occurs

in real life. Bottomhole pressure and reservoir pressure change dynamically, and because of this change, fluid inflow rates change affecting the onset of liquid loading, as liquid flow rate increases with time.

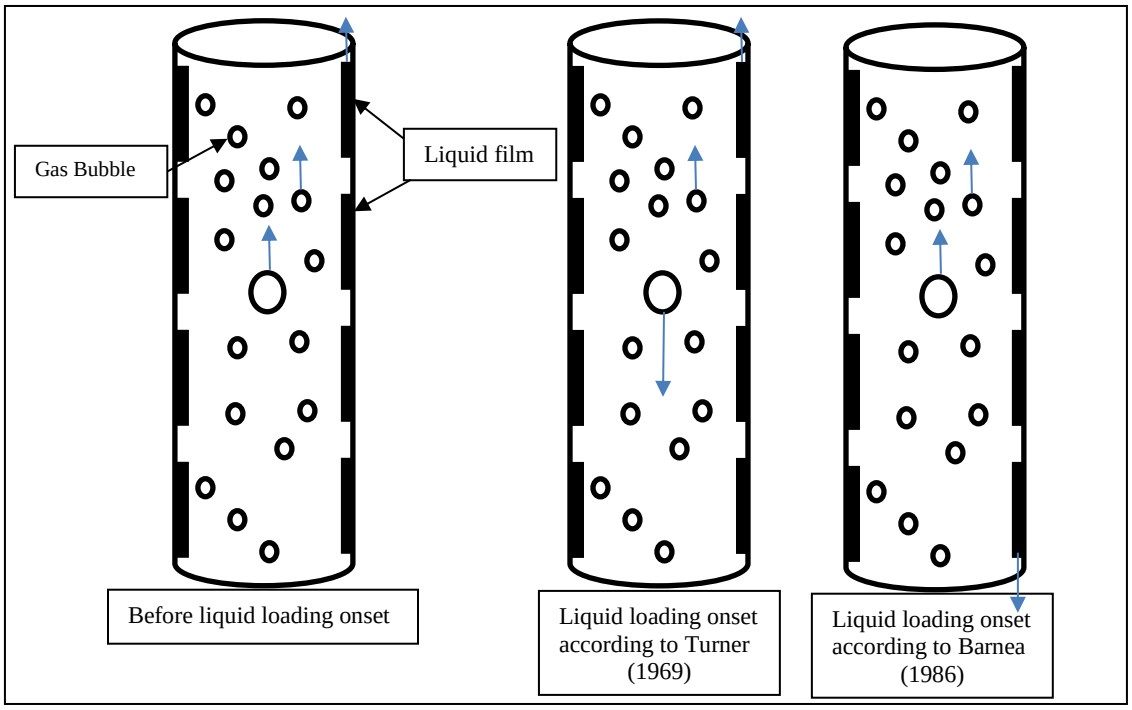

Figure 1 Liquid loading onset criteria based on the most two known theories.

Modeling liquid loading has been for a long time an issue linked to the wellbore only. Most of the published studies focused, as a result, on the wellbore to study the phenomena. The studies focused on the transition from annular flow to churn or slug flow as the onset of liquid loading Figure 1. In other words, flow pattern recognition was considered the key (Pushkina and Sorokin 1969; Zapke and Kroeger 2000; Hewitt 2012).

Critical gas velocity concept is one of the main terminologies developed in this matter. This concept is a function of both densities value, developed by Turner et at. (1969). The equation has been modified slightly by the industry as more data became available. The critical gas velocity developed by Turner is corrected with 16%.

The liquid associated with the gas flow has been attributed to the water or hydrocarbon condensate or both coming from the formation (Sutton et al. 2010; Wang et al. 2010; Zhou and Yuan 2010). Recent studies went further into studying the liquid loading in the wellbore with experiments and translucent pipes aided with high-speed cameras capturing the flow pattering continuously. The results of these studies suggest that the liquid film coating the tubing breaks first and should be studied (Van't Westende et al. 2007; Veeken and Belfroid et al. 2011; Waltrich and Barbosa et al. 2011; Alamu et al. 2012; Luo et al. 2014)

Liquid loading phenomena are complicated. Studying the wellbore is not enough. It involves the reservoir and the wellbore. The multiphase flow is not just inside the wellbore; it is a two-phase flow from the reservoir presenting a complexity to any researcher looking into this matter. Coupling the wellbore model with a reservoir model can enhance our understanding of the liquid loading phenomena.

Riza et al. (2016) have developed a coupled wellbore-reservoir model studying the onset of liquid loading along the entire wellbore. The issue here is again the focus on the wellbore only. The flow coming from the reservoir is very simplistic IPR approach. Limpasurate and Valko et al. (2015) developed a coupled model as well, using a reservoir model to handle the flow coming from the reservoir. An elegant model that detects the crossflow from the wellbore into the formation.

The above mentioned two models are a significant step in understanding the whole phenomena. However, both approaches have shortcomings.

Simplistic reservoir Inflow Performance Relationship equation coupled with mechanistic model in the wellbore with the assumption of fixed reservoir pressure and constant drop rate at the bottom of wellbore, and using constant gas oil ratio to determine liquid phase flow rate, is

inaccurate approach though can give us a glimpse of how flow pattern changes throughout the entire wellbore and that is what we have learned from Riza et al. (2016). He noticed that the onset of liquid loading begins at the bottom of the wellbore before anywhere.

Limpasurate and Valko et al. (2015) model, on the other hand, presented a sophisticated model to study the liquid loading using a coupled approach. As much as their model provided a definite possibility of the cross-flow between the wellbore and the formation, it is a complicated approach in every aspect. They utilized a transient reservoir simulation model, which requires specialized training to be programmed. Not to mention that they did not provide steps on how to recreate their model.

Finally, we can see the need for a new approach. It should be realistic yet with fewer complications so that it can be executed on any computer software. Table 1 provides a comparison between the current models and the proposed model.

Table 1 Coupled models comparison

	Riza et al. (2016)	Limpasurate and Valko et al. (2015)	Proposed Model
Simplicity	Yes	No	Yes
Reservoir simulation	No	Yes	No
Mechanistic Wellbore Model	Yes	Yes	Yes
Easy to program	Yes	No	Yes
Dynamic	No	Yes	Yes
Can be used to study wellbore two-phase flow	No	No	Yes
Varying liquid phase flow rate	No	Yes	Yes

Reservoir pressure and bottomhole pressures change dynamically depending on reservoir properties and the drawdown. In the wellbore-reservoir connected systems, the only constant pressure is the wellhead pressure. Controlling wellhead pressure affects the downhole pressure directly and ultimately the decline rate of reservoir pressure. Reservoir system is very complicated. Production engineers tend to approach the whole wellbore-reservoir coupled model in a simplified way by using a single IPR equation and several assumptions. Other researchers with reservoir engineering background, they implement reservoir numerical simulation to handle the reservoir system and couple it with wellbore pressure drop system. Other researchers implement fully fledged commercial reservoir simulator to handle the reservoir aspect and another specialized production simulator as the coupled model presented in the validation section where they used a commercial simulator called MoRes a property belongs to Shell for the reservoir and Olga to handle wellbore pressure drop calculations. Reservoir modeling is not as easy as wellbore modeling because it is not a very well-defined medium. In the wellbore, we have a specific medium shape with fixed geometry for the fluid to flow. On the other side, the

reservoir shape is usually assumed to be circular. Besides, the medium in which the fluid flows is nonhomogeneous. Permeability and porosity are significantly different in each reservoir area. Reservoir engineers utilize the power of reservoir simulators to discreet reservoir bulk volume into smaller grids. For each gird, they assign rock and fluid properties. This task requires deep reservoir flow and simulation knowledge. This approach has been adopted by Valko et al. (2015). They took advantage of open source code for reservoir simulator developed at Texas A&M University to handle the reservoir system. As for the wellbore, they used Turner et. Al. (1967) critical flow equation to determine the onset of liquid loading.

CHAPTER II

METHODOLOGY

Building a wellbore-reservoir coupled simulation requires the use of different models and correlations from both reservoir and production fields. The simulations consist of two systems incorporating together. The reservoir system and the production system. A step by step procedures will be given to be able to program the simulation. This large simulation requires the use of several loops and implicit equations. It should be implemented with the aid of any computer program. The input data required for the simulation is given in Table 2.

Table 2 Simulation input data

Reservoir Data	Wellbore Data	Stream Data
Reservoir initial pressure	Wellhead pressure	Gas critical temperature
Reservoir initial temperature	Wellhead temperature	Gas critical pressure
Reservoir area	Tubing diameter	Gas specific gravity
Reservoir permeability	Pipe roughness	Water density
Reservoir thickness	Wellbore deviation angle	
Reservoir porosity	Wellbore diameter	
Reservoir saturation	Wellbore depth	

Reservoir System Modeling

The flow of the simulation is carried away in the following order. First, the gas flow rate and water flow rate are calculated from the reservoir initial given properties.

$$q_g = \frac{\left(p^2 - p_{wf}{}^2\right)k_g h}{1{,}424\,\mu_g z(T+460)\ln(0.472\,r_e / r_w)} \quad (3)$$

$$q_w = \frac{k_w h(p - p_{wf})}{141.2 B_w \mu_w \ln(0.472\,r_e / r_w)} \quad (4)$$

q_g : Gas flow rate, MSCF/d

q_w : Water flow rate, STB/d

p : Reservoir average pressure, psi

p_{wf} : Bottomhole flowing pressure, psi

k_g : Gas effective permeability, md

h : Reservoir thickness, ft

μ_g : Gas viscosity, cp

T : Reservoir temperature, ^{o}F

r_e : Reservoir radius, ft

r_w : Wellbore radius, ft

Gas and liquid effective permeabilities are required to calculate the flow rates from Eq.1 and Eq.2, both phases effective permeabilities are required. If only one phase exists, the use of absolute permeability should be sufficient. However, since two phases are flowing in the pours medium, each phase is competing against each other to flow. As a result, the flow rate for each phase is less compared to only one phase. This issue was solved by using the concept of relative permeability. It means that each phase is only flowing through a fraction of the absolute permeability. This fraction is called the effective permeability. In other words, relative permeability is the ratio of the effective permeability to the absolute permeability. Calculating

relative permeability is a tricky task as it involves reservoir lithology and rock wettability. Many researchers introduced relative permeability curve correlations. However, most of these correlations are derived for water flooding reservoir in which initial water saturation is considered irreducible. Also, water saturation increases with time as more water is being injected into the reservoir. These correlations cannot be utilized in our simulation to calculate both phases effective permeabilities. In our model, the only source of water is the initial water in place. In other words, the initial water is producible, and water saturation decreases with time as the production process continues.

Relative permeability correlations should be tuned to be able to use them in this situation. Modified Brooks and Corey model et al. (1966) is one of the most used models in the oil and gas industry. Eq. 5 is used to calculate gas relative permeability and Eq. 6 is used to calculate water relative permeability. Since the initial water is producible based on our assumption, initial water saturation in Eq. 6 is changed to irreducible water saturation Eq. 7.

$$k_{rg} = \left(\frac{1 - s_w - s_{gr}}{1 - s_{gr}} \right)^2 \quad (5)$$

$$k_{rw} = \left(\frac{s_w - s_{wr}}{1 - s_{wi}} \right)^2 \quad (6)$$

$$k_{rw} = \left(\frac{s_w - s_{wr}}{1 - s_{wr}} \right)^2 \quad (7)$$

$$k_g = k_{rg} k \quad (8)$$

$$k_w = k_{rw} k \quad (9)$$

k_{rg} : Gas relative permeability, md

k_{rw} : Water relative permeability, md

s_w : Water saturation

s_{wr} : Irreducible water saturation

s_{gr} : Residual gas saturation

Gas residual saturation is needed to calculate gas relative permeability. Gas residual saturation is the amount of gas in the reservoir at abandonment pressure. In other words, the amount of gas that cannot be produced when reservoir energy represented by reservoir pressure is severely depleted and cannot lift the fluids anymore to the surface. Gas residual saturation depends on rock lithology and wettability. Agarwal et al. (1967) developed an empirical correlation to predicate gas residual saturation for common rock categories based on experimental data Eq. 10.

$$S_{gr} = 0.1813 S_{gi} + 0.096071 \quad (10)$$

s_{gr} : Residual gas saturation

s_{gi} : Initial gas saturation

The previous paragraphs illustrating the process of determining the relative permeabilities for both phases. However, it would be impossible to get values for water saturation. As a result, in the proposed model, relative permeabilities initial values are provided by the user.

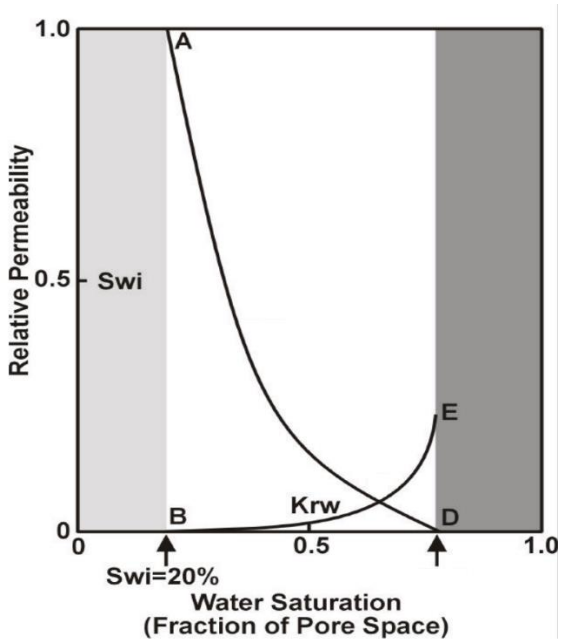

Figure 2 Typical plot for gas-water relative permeability relationship

The user is required to input the values of A, B, E, and D as illustrated in figure 2. A is the initial gas saturation. B is the initial water saturation. E is the irreducible water saturation. D is the residual gas saturation.

The proposed model gives the user the option of using the initial values of relative permeabilities in the calculation or utilize the built in exponential function to construct a curve matching the user core lab relative permeability data. The built-in equation is

$$k_{rw} = ne^{mS_w}$$

The default values for n and m are 0.002 and 6.5 respectively. These values can be modified as well by the user. As for the gas relative permeability the following equation is utilized.

$$k_{rg} = ne^{mS_w}$$

The default values for n and m are 8.11 and -8.4. the values can be modified by the user as well.

Wellbore System Modeling

One more essential parameter is needed before calculating gas and water flow rate coming from the reservoir into the wellbore, bottomhole pressure. For any fluid to flow in any medium, there must be a pressure difference. In any reservoir-wellbore coupled model, there are two central pressures. One is the reservoir pressure representing reservoir energy. The other pressure is the bottomhole pressure. The bottomhole pressure is the common point between the reservoir system and the wellbore system. Based on the philosophy of nodal analysis, there must be one value of bottomhole pressure that can satisfy both the reservoir system and the wellbore system. Ideally, zero bottomhole pressure is favorable as it produces the most hydrocarbon based on Eq. 3. If zero bottomhole pressure can be achieved, will the fluid be able to travel all the way from the bottom of the wellbore to the surface? Again, the pressure difference must exist for fluids to flow. Since the wellhead pressure cannot be lowered less than the atmospheric pressure, the maximum hydrocarbon flow rate at zero bottomhole pressure cannot be achieved.

There are three main issues to be considered for fluids to flow from the bottom of the well up to the surface. The hydrostatic pressure loss caused by the column of fluid density inside the well. The friction pressure loss and the wellhead pressure which must meet the sale line pressure. The wellhead pressure should be high enough for the fluid to flow to the last destination. Now the main question remains unanswered, what is the value of bottomhole pressure that should be used in Eq. 3 and Eq. 4 and satisfy both, the reservoir and the wellbore system?

The first time the simulation starts to run, it will assume any value less than the reservoir pressure to create a fluid flow, have both gas, and water fluids rate. Eq. 11 is applied to have arbitrarily assumed bottomhole pressure.

$$p_{wf,assumed} = \bar{p}_R - 200 \quad (11)$$

$p_{wf,assumed}$: Assumed bottomhole pressure, psi

$\bar{p}_R$: Reservoir average pressure, psi

Eq. 3 and Eq. 4 can now be run with the aid of given reservoir properties, the calculated relative permeabilities, and the assumed bottomhole pressure. Before going into the next step, both gas and water flow rates should be converted into velocities as the upcoming equations rely on them.

Now, we can back-calculate bottomhole pressure from wellhead pressure. Wellhead pressure is always known as it should meet the sales line pressure. In our case, wellhead pressure is set to 300 psi. The idea behind recalculating bottomhole pressure from wellhead pressure is to validate our initial bottomhole pressure assumption. In other words, one point cannot have two different pressures at the same time.

Converting the fluid flow rates to velocities will make the next set of calculation much more manageable. The velocity is the ratio of fluid flow rate to the area. Since two-phases are flowing inside the wellbore, calculating the exact velocity requires knowing the exact area each fluid occupies. This task is extremely complicated. Instead, the concept of superficial velocity is used. The superficial velocity concept ignores the fact that two-phases are flowing at the same time. In other words, to obtain the superficial velocity for any phase, the flow rate is divided by the whole pipe area. The following velocity equations are presented in in-situ conditions (reservoir conditions), hence the use of formation volume factors.

$$v_{sl} = \frac{5.615}{86400} q_w B_w \quad (12)$$

$$v_{sg} = \frac{1000}{8600}\frac{q_g B_g}{a} \quad (13)$$

$$a = \frac{\pi}{4} d^2 \quad (14)$$

v_{sl} : Superficial liquid velocity, ft/sec

v_{sg} : Superficial gas velocity, ft/sec

q_w : Water flow rate, STB/d

q_g : Gas flow rate, MSCF/d

B_w : Water formation volume factor, bbl/STB

B_g : Gas formation volume factor, cu ft/SCF

a : wellbore area, ft^2

d : Wellbore diameter. ft

Bottomhole Pressure Reverse Calculation from Wellhead Algorithm

Wellbore in the simulation is segmented into 100 segments. Bottomhole pressure can be calculated in one long segment, from the wellhead down to the bottomhole. However, considering the whole wellbore as one segment yields a significant error in calculating bottomhole pressure. The reason behind this is the change of fluid properties with elevation. Fluid properties change with temperature and pressure. To minimize the error resulted from the properties change, the wellbore is segmented into small segments. We start from the wellhead and calculate the pressure at the bottom of the first segment. This pressure is used again to calculate the pressure at the bottom of the next segment and so on. Figure 3 illustrates the segmenting process. The process starts with calculating the first segment bottom pressure.

$$p_1 = p_{wh} + \Delta p_1 \quad (15)$$

p_1 : Pressure at the bottom of top segment, psi

Δp_1 : Pressure drop the top segment, psi

p_{wh} : Wellhead pressure, psi

Pressure drop Δp_1 consists of two main components, friction loss, and hydrostatic pressure loss.

$$\Delta p_1 = \left[\frac{\Delta p_f}{L} + \frac{\Delta p_h}{L} \right] L \quad (16)$$

$\frac{\Delta p_f}{L}$: Pressure gradient due to pressure, psi/ft

$\frac{\Delta p_h}{L}$: Pressure gradient due to hydrostatic pressure, psi/ft

Δp_1 : Pressure drop across the segment, psi

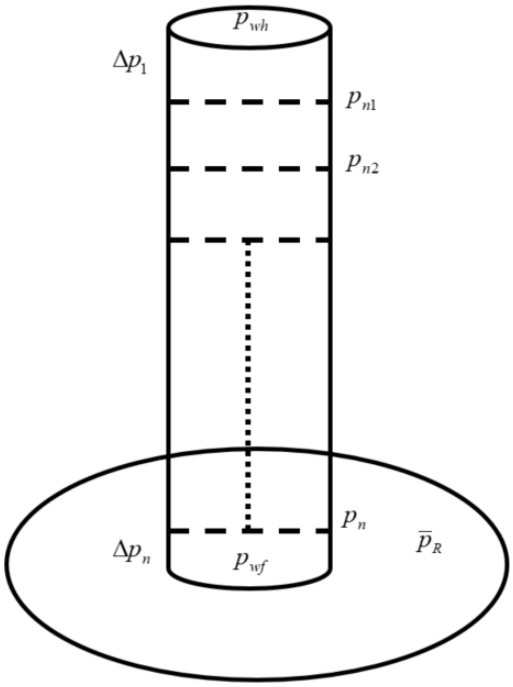

Figure 3 Wellbore segmented approach

To calculate both pressure drop due to friction and hydrostatic pressure, fluid properties are needed. If only a single phase is flowing inside the wellbore, calculating fluid properties would be much more comfortable. In contrary, two-phase flow presents greater difficulty. Which fluid properties should be used to calculate the pressure losses? The answer is both phases properties should be utilized. To do it, a crucial parameter in the two-phase calculation should be introduced, liquid holdup. It answers how much liquid is occupying any segment in the wellbore which is very important because we can know which phase is dominating in any segment. The liquid holdup is the ratio of the volume of liquid to the volume of the pipe segment. In other words, it gives the parentage of both phases occupying the wellbore segment. According to these percentages, mixture properties are calculated. Eq. 17 gives mixture density in lb/ft^3 and Eq. 18 gives mixture viscosity.

$$\rho_m = f_g \rho_g + f_l \rho_l \quad (17)$$

ρ_m : Mixture density, lb/ft^2

ρ_g : Gas density, lb/ft^2

ρ_l : Liquid density, lb/ft^2

f_g : Void fraction factor

f_l : Liquid holdup factor

$$\mu_m = x\mu_g + (1-x)\mu_l \quad (18)$$

μ_m : Mixture density, cp

μ_g : Gas density, cp

μ_l : Liquid density, cp

Reservoir gas and water viscosity in cp unit is calculated by Lee et al.

$$\mu_g = A10^{-4} EXP\left(B\rho_g^C\right) \quad (19)$$

$$A = \frac{(9.4 + 0.02M)T^{1.5}}{(209 + 19M + T)} \quad (20)$$

$$B = 3.5 + 0.01M + \frac{986}{T} \quad (21)$$

$$C = 2.4 - 0.2B \quad (22)$$

$$\mu_w = \exp\left(1.003 - 1.479 \times 10^{-2} T + 1.982 \times 10^{-5} T^2\right) \quad (23)$$

The parameter x in Eq. 18 is another dimensionless parameter that quantifies the gas phase in the fluid mixture. It can be calculated with Eq. 24

$$x = \frac{v_{sg}\rho_g}{v_m\rho_m} \quad (24)$$

$$\rho_g = \frac{pM_w}{zR(T + 460)} \quad (25)$$

T: Temperature, ^oF

p : Pressure, psi

As for the liquid holdup needed in Eq. 17, there are several ways to obtain it. A few of those ways have discussed in the literature review chapter. In this study, Hasan-Kabir model is implemented to calculate the liquid holdup. The reason is, the H-K model considered one of the simplest models among the mechanistic models which are known for their complexity.

Calculating the liquid holdup requires the determination of flow pattern in the wellbore segment. The flow pattern is the distribution of the two phases inside the pipe segment. For vertical wells, there are four distinct flow patterns, bubbly flow, slug flow, churn flow, and annular flow.

Some parameters are required to check the flow pattern. These parameters are a function of fluid properties. All velocities are in ft/sec.

$$c_o = 1.15\left(1-\exp\left(-0.2\frac{v_{gc}}{v_{sg}-v_{gc}}\right)\right)+\exp\left(-0.2\frac{v_{gc}}{v_{sg}-v_{gc}}\right) \quad (26)$$

$$v_{\infty T\alpha} = 0.35\left(gD\left(\frac{\rho_l-\rho_g}{\rho_l}\right)\right)^{0.5} F_\alpha F_a \quad (27)$$

$$F_\alpha = (1+\cos\alpha)^{1.2}(\sin\alpha)^{0.5} \quad (28)$$

$$F_a = 1+0.286\left(\frac{d_i}{d_o}\right) \quad (29)$$

$$\bar{v}_\infty = v_{\infty b}\left(1-\exp\left(-0.1\frac{v_{gb}}{v_{sg}-v_{gb}}\right)\right)+v_{\infty T\alpha}\exp\left(-0.1\frac{v_{gb}}{v_{sg}-v_{gb}}\right) \quad (30)$$

v_{sl} : Superficial liquid velocity, ft/sec

v_{sg} : Superficial gas velocity, ft/sec

v_{gc} : Critical gas velocity, ft/sec

d : Pipe diameter, ft

α : Wellbore inclination angle, degree

The simulation first calculates annular transition velocity, which is the minimum gas velocity, required for the flow to be considered annular flow.

$$v_{gc} = 3.1\left(0.0022048\, g\sigma_w\frac{\rho_l-\rho_g}{\rho_g^2}\right)^{0.25} \quad (31)$$

v_{gc} : Critical gas velocity, ft/sec

ρ_l : Liquid density, lb/ft^3

ρ_g : Gas density, lb/ft^3

σ_w : Water-gas interfacial tension, dynes/cm

If the superficial gas velocity in the wellbore segment is above the value obtained in Eq. 31, the flow is considered annular flow. If the gas velocity is less than Eq. 31, the simulation checks for bubbly flow.

$$v_{\infty b} = 1.53\left(g\left(\frac{\rho_l - \rho_g}{\rho_l^2} \right)\sigma_w 0.0022048 \right)^{0.25} \quad 32$$

ρ_l : Liquid density, lb/ft^3

ρ_g : Gas density, lb/ft^3

σ_w : Water-gas interfacial tension, dynes/cm

If the gas velocity in the streams is less than the value obtained from Eq. 32, the flow pattern is bubbly flow. If not, the program proceeds to check churn flow.

$$v_{\infty a} = 1 - \exp\left(-0.01 \frac{v_{gc}}{v_{sg} - v_{gc}} \right) \quad 33$$

Water-gas interfacial tension, dynes/cm, does not have a significant effect on two-phase calculations. However, their values are needed for the sake of calculation.

$$\sigma_{w(74)} = 75 - 1.108\, p^{0.349} \quad 34$$

$$\sigma_{w(280)} = 53 - 0.1048\, p^{0.637} \quad 35$$

$$\sigma_{w(T)} = \sigma_{w(74)} - \frac{(T - 74)\left(\sigma_{w(74)} - \sigma_{w(280)}\right)}{206} \quad 36$$

p : Pressure, psi

$\sigma_{w(74)}$: Water gas interfacial tension at 74 ^{o}F

$\sigma_{w(280)}$: Water gas interfacial tension at 280 ^{o}F

If the gas velocity in the wellbore segment is less than Eq. 37, the flow pattern is considered bubbly flow.

$$v_{gb} = (0.43v_{sl} + 0.36v_{\infty b})\sin(\theta) \quad (37)$$

If flow pattern has been determined successfully, liquid hold up and gas void fraction can be calculated with Eq. 38 and Eq. 39. Model coefficients are shown in Table 3.

$$f_g = \frac{v_{sg}}{c_o v_m + v_\infty} \quad (38)$$

$$f_l = 1 - f_g \quad (39)$$

Table 3 Hasan-Kabir model coefficients

Flow Pattern	Flow Parameter C_o	Rise Velocity, v_∞
Bubbly Flow	1.2	$v_{\infty b}$
Slug	1.2	$\bar{v}_\infty$
Churn	1.15	$v_{\infty T\alpha}$
Annular	1	0

After determining liquid hold up, mixture density can be calculated from Eq. 17. Hydrostatic pressure drop can now be calculated as well.

$$\frac{\Delta p_h}{L} = \frac{\rho_m}{144}\sin\alpha \quad (40)$$

Δp_h : Hydrostatic pressure loss, psi

ρ_m : Mixture density, lb/ft^3

L : Length, ft

α : Well inclination angle, degree

Friction pressure drop is the main contributor to pressure loss in gas wells as gas density is very low yielding a low hydrostatic pressure, but a high gas velocity leads to a high friction loss.

$$\frac{\Delta p_f}{L} = \frac{f v_m^2 \rho_m}{2*144 d g_c} \quad (41)$$

Δp_f : Friction pressure loss, psi

d : Pipe diameter, ft

The friction factor is required to calculate the pressure drop due to friction. Friction factor shows how rough the pipe walls are. Reynolds number for field unit is calculated with Eq. 43

$$f = 0.001375\left(1+\left(20000\,\frac{\varepsilon}{d}+\frac{10^6}{\mathrm{Re}_n}\right)^{1/3}\right) \quad (42)$$

$$R_{en} = \frac{\rho_m v_m d}{0.000672\,\mu_m} \quad (43)$$

ρ_m : Mixture density, lb/ft^3

v_m : Mixture velocity, ft/sec

d : Pipe diameter, ft

B_{gi} : Gas formation volume factor, ft^3/SCF

Total pressure drop is then calculated with Eq. 16. The calculated pressure drop is for one segment only of the wellbore. From Eq. 15, the pressure at the bottom of the first segment are obtained. The calculation should be carried to the next segment. Starting from the recently obtained pressure, the pressure drop in the next segment is calculated. The same process is repeated until bottomhole pressure is calculated. We need to remember that all the previous

calculations were based on fluids flow rate obtained from a guessed bottomhole pressure. Since this is the first iteration, obviously the calculated value of bottomhole pressure is not equal to the guessed value. As a result, a convergence equation is needed to obtain a new guess Eq. 44.

$$p_{wf} = 0.5\,p_{wf,wh} + 0.5\,p_{wf,\mathrm{Re}} \qquad 44$$

$p_{wf,wh}$: Bottomhole pressure calculated backward from the wellhead, psi

$p_{wf,wh}$: Bottomhole pressure calculated from the reservoir, psi

This process must be automated as it takes hundreds of run to find the correct bottomhole pressure which satisfies both the reservoir and wellbore system with one psi error margin. The obtained bottomhole pressure represents the pressure at the end of the first day of production. The time step can be specified by the simulation user; however, in our base case run, the time step is set to one day. The next step is to figure out the new reservoir pressure for the next day. First, gas in place volume is calculated volumetrically.

$$G_i = \frac{43{,}560\,Ah\phi(1-s_{wi})}{B_{gi}} \qquad 45$$

$$B_{gi} = 0.0283\frac{(460+T)z_i}{p} \qquad 46$$

G_i : Initial gas in place, SCF

Ah : Area-Thickness, acres-ft

B_{gi} : Initial gas formation volume factor. ft^3/SCF

T : Temperature, ^oF

The flow rate obtained from Eq. 3 represents the volume of gas obtained in one day. If we subtract the produced gas from the original gas in place, we get the remaining gas in place.

Rearranging Eq. 3 and using the remaining gas in place, the new water saturation, or the reservoir water saturation for the next day can be calculated

$$s_{wi} = 1 - \frac{(G_i - G_p)B_g}{43{,}560\,Ah\phi} \quad (47)$$

$$G_p = q_g \times 1000 \quad (48)$$

G_p : Cumulative gas production, SCF

q_g : Gas flow rate, MSCF/d

Gas formation volume factor is calculated at the new reservoir pressure. Up until this point, we are seeking the new reservoir pressure which can be calculated by the dry gas reservoir material balance.

$$p = \frac{p_i}{z_i}\left(1 - \frac{G_p}{G_i}\right)z \quad (49)$$

p : Reservoir pressure, psi

p_i : Initial reservoir pressure, psi

As can be seen from Eq. 49, gas reservoir compressibility factor at the new reservoir pressure is required that is one equation with two unknown parameters. To solve this dilemma, a new assumption is made. Since reservoir pressure cannot change that much in one day, it is safe to assume that, the gas compressibility factor for the previous day is still applicable. For each run, the previous-day gas reservoir compressibility factor will be used to acquire the new reservoir pressure.

After acquiring the new reservoir pressure, a new guess for the bottomhole pressure will be made, and the whole process is repeated all over again until the well dies either due to water loading or insufficient reservoir pressure.

CHAPTER III

MODEL VALIDATION

In this chapter, the proposed model is validated with commercial software simulation and field data. The model runs a set of data from a study done in Norway utilizing Olga for the wellbore calculation, and a reservoir simulation belongs to Shell. They used the same approach as in this study by implementing two systems to create a coupled wellbore-reservoir model.

Then the model will be utilized to study liquid loading phenomena. The study will focus on flow pattern changes inside the wellbore. The flow pattern change from the annular flow is the trigger of liquid loading onset. The moment the gas velocity drops below the annular transitional velocity, gas will not be able to lift liquid droplets to the surface. As a result, bottomhole pressure starts to buildup decreasing drawdown pressure, hence decreasing the gas flow rate. To investigate the liquid loading phenomena properly, flow pattern throughout the entire wellbore should be observed.

The model can produce a dynamic image for the entire wellbore on a previously set time step. This image provides a better look at what takes place inside the wellbore. For a gas well, typically the flow pattern on early days of production is annular flow. As reservoir pressure depletes, flow pattern changes to slug or churn flow before it ultimately dies due to liquid loading. The model can detect the onset of liquid loading anywhere inside the wellbore. Besides, the life expectancy for the well is reported. Knowing ahead of time, the time at which liquid loading occurs, allow the operating company to intervene to delay the onset of liquid loading and as a result, extend the well-life.

Validation Against Commercial Software

In this section, the proposed model is validated against data set obtained from a study published under the title "Simulating liquid loading in gas wells," W. Schiferil et al. 2010. The data is presented in Table 4.

Table 4 Validation data set obtained from the literature

Reservoir			Wellbore			Stream		
p_i	4,351	psia	p_{wh}	290	psia	T_{pc}	378	^oR
T	212	^oF	T_{wh}	129.2	^oF	p_{pc}	671	psia
A	218	acres	d	3.5	in	MW	17.53	lbm/lb mole
k	5	md	Ɛ	6.00E-03	ft	γ_g	0.6	
h	328	ft	θ	90	^{o}			
φ	0.12		r_w	0.46	ft			
S_{wi}	0.25		Depth	9,842	ft			

The noticeable parameter from the provided set of data is reservoir thickness. The reservoir under investigation is a massive reservoir with over 300 ft of thickness. Moreover, the reservoir is considered deep as well, with over 9000 ft. According to the study, this well is expected to die on day 3,191 after production starts. The gas flow rate at abandonment pressure was reported to be 0.6 MMSCF/day with a water flow rate of 14 bbl/day.

The same data was used as an input in our proposed model. The output data is presented graphically in Figure 5.

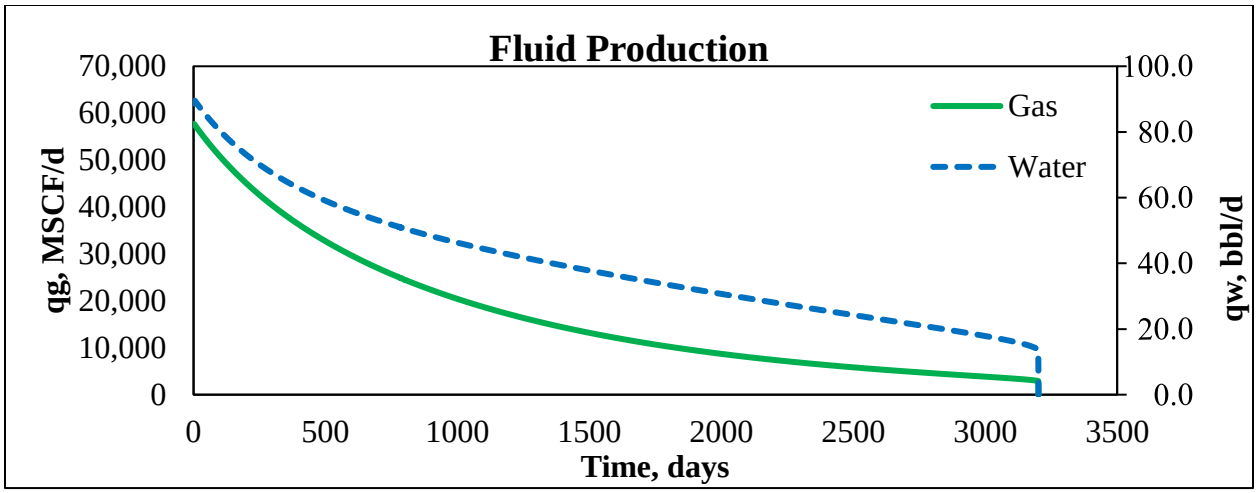

Figure 4 Gas and water flow rate based on input data acquired from a published study (W. Schiferil et al. 2010)

Figure 4 shows the decline of both fluids flowrate over time as reservoir depletes. The last day of production is 3,212 as it can be seen from Figure 4. This value agrees with the one obtained from the use of fully-fledged commercial simulation. The gas and water flow rates match the simulation reasonably. The results are tabulated in Table 5.

Table 5 Comparison between the proposed model and reservoir-wellbore commercial software

	OLGA & Shell	Our Model
Well Life, day	3187	3202
Last Water Flow Rate, bbl/day	14	14
Last Gas Flow Rate, MMSCF/day	2.8	2.9

Tables 5 proves the validity of the proposed model. Using commercial software requires specialized training as well as owning the license to use it in the first place which gives the proposed model a reasonable advantage over the commercial simulations. Also, the use of commercial software restricts the user to limited correlations and narrows the usage to what is

already installed in the package. The proposed model, which was explained step by step, can be modified in any way the researchers want. Any correlation, whether it was used for fluid properties of calculating income flow rate or even the mechanistic wellbore pressure drop can be changed. The model is designed in a way to give the user the full power to adopt any approaches to study wellbore issues. For example, horizontal-well inflow equation can replace the current inflow equation for a vertical well. Moreover, using gas well reservoir material balance instead of dry gas material balance would allow the study of oil and water holdup in the wellbore bearing in mind that, using a complicated approach like gas wet material balance mandates the implementation of three fluid inflow equations and their respective relative permeability curve equations. Since the model can be versatile, it would be beneficial in the academia among petroleum engineering students.

The total run time to validate our model with the commercial software data was 5 minutes. If commercial software is intended to be used for its superior accuracy, the proposed model can be used first to get a preliminarily results before running the commercial software. This will save the company a tremendous amount of time as it gives the engineers an estimate of the course of actions or the consequences of their input data.

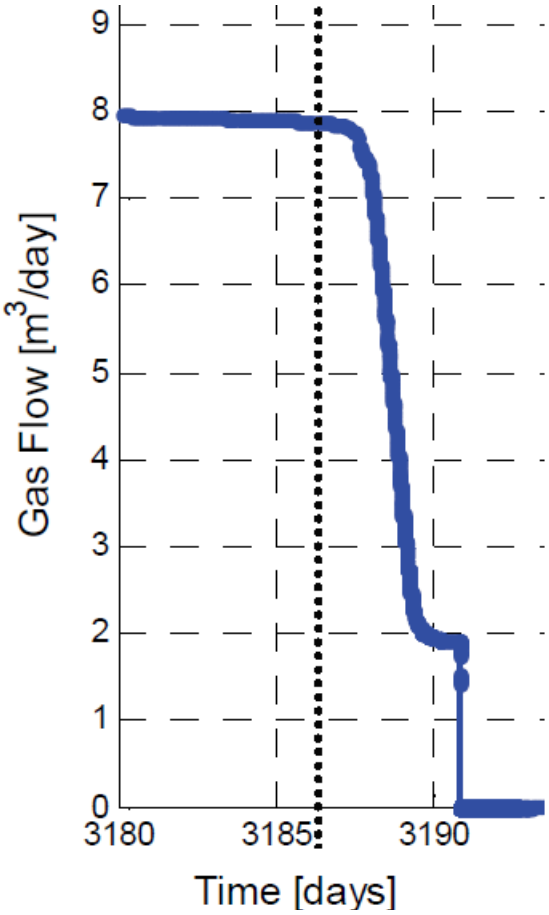

Figure 5 Olga and reservoir simulation results in SI units

Studying Figure 6 shows the gas flow rate decline suddenly to a little value. Then, within one day the well-flow rate becomes zero. Because they were utilizing a commercial reservoir software, the simulation is dealing with the reservoir as a unit built with different grid properties. Unlike the model presented in this study, which considers the reservoir as a one big grid block, they were able to capture the well's final hours. Nevertheless, having a one-day error in exchange for a simulation completing years run within 3 minutes is a reasonable compromise.

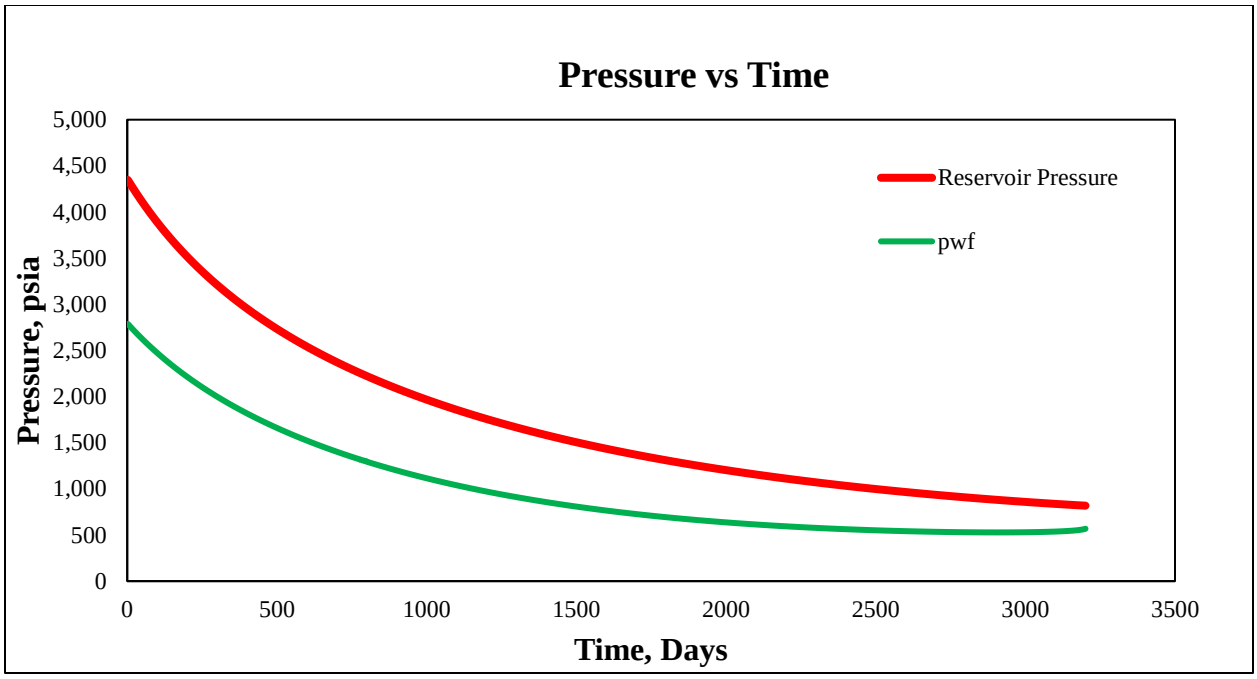

Figure 6 Pressure data from our simulation for the Norwegian case simulated by our model

Unfortunately, reservoir pressure data is not presented in the Norwegian case. We tried to obtain the reservoir and bottomhole pressures with our model. The result is presented in Figure 7. Both pressures are declining with production. However, the point which deserves our attention is the absence of the sudden increase of buttonhole pressure. The sudden increase of the buttonhole pressure is a sign of liquid accumulation at the bottom of the well, hence the effect of liquid loading. In contrary, the will dies as the reservoir pressure is insufficient to move the fluid into the wellbore. In other words, it is a reservoir problem, not a wellbore problem and surely not a liquid loading problem.

In some gas wells, the well dies because of the reservoir pressure depletion but liquid loading is reported as the reason for the death. Another set of data is needed to decide for sure. Liquid holdup profile at the bottom of the well throughout the life of the well should shed more light on this issue. Figure 8 displays liquid holdup profile.

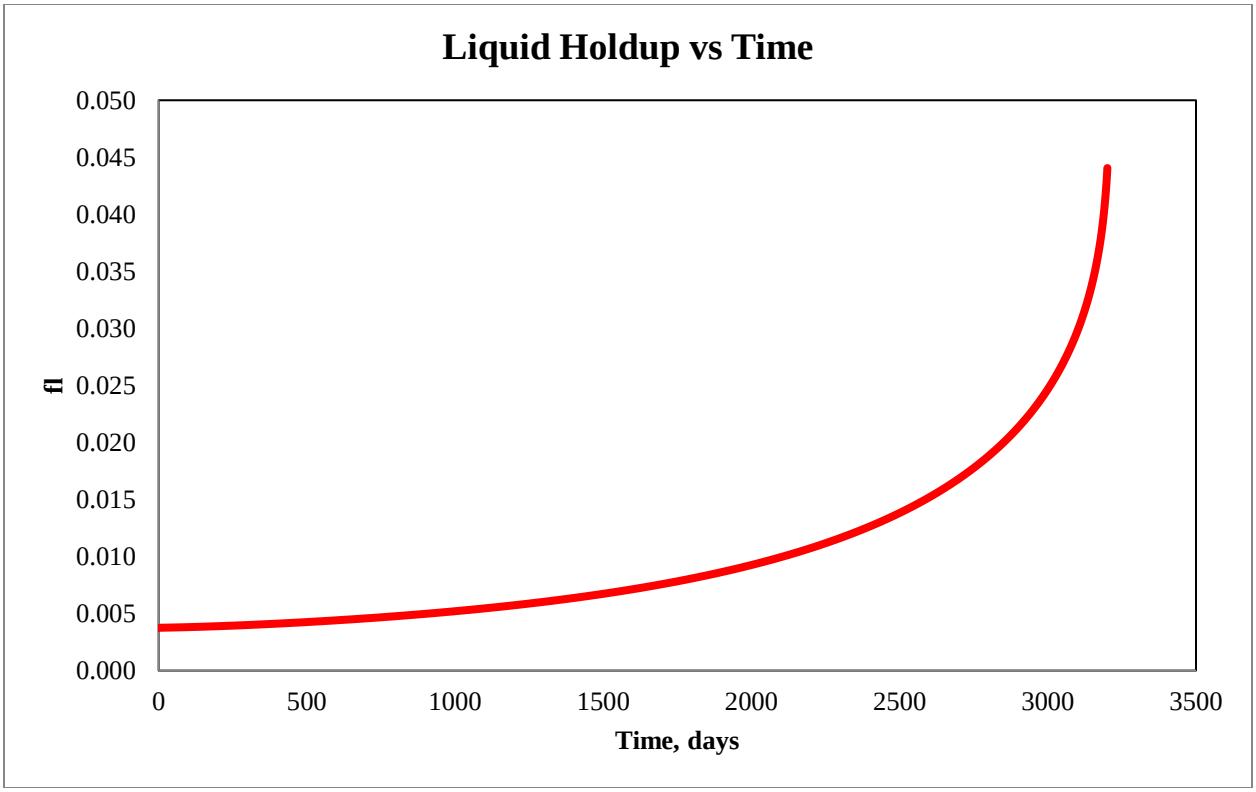

Figure 7 Liquid holdup profile at the wellbore bottom throughout the well's life

From Figure 8, the liquid holdup increases exponentially with time which means more liquid is accumulating at the bottom of the well, but still not enough to be considered a liquid loading problem. The well is going in the direction of liquid loading as the gas flow rate decreases with time. The maximum value of liquid holdup is less than 0.05 on the last day of production. Because of this, the well dies from reservoir pressure depletion, not from liquid loading.

Validation Against Field Data

Table 6 Field data rearranged and modified from (Li et al. 2002)

Well	Producing Depth, *ft*	Wellhead Pressure, *psi*	Water Prod. *bll/d*	Gas Prod. ft^3/d	Production Statue	z Factor	Proposed Model	Water Prod. *bll/d*	Gas Prod. ft^3/d
1	7,569	2,234	2.20	1,214,614	Unloaded	0.836	Unloaded	1.7	1,119,037
2	6,578	1,740	2.39	1,197,663	Unloaded	0.848	Unloaded	1.73	1,128,229
3	7,894	3,162	7.86	1,591,492	Unloaded	0.847	Unloaded	7.5	1,508,291
4	7,802	2,393	5.03	1,687,336	Unloaded	0.835	Unloaded	5.4	1,737,640
5	9,875	2,263	4.40	1,655,730	Unloaded	0.836	Unloaded	4.81	1,571,44
6	8,720	3,350	7.55	1,612,822	Unloaded	0.849	Unloaded	8.2	1,655,530
7	8,163	2,857	14.47	1,765,735	Unloaded	0.54	Unloaded	8.6	1,734,977
8	8,743	2,582	7.86	358,091	Unloaded	0.839	Unloaded	6.73	352,205
9	7,677	2,611	28.30	318,892	Load-up	0.839	Loaded	18.4	305,226

Tubing inside diameter is 2.44 in. Temperature is 120 F. Gas gravity is 0.6. Table 6 shows field data rearranged and modified from (Li et al. 2002), for gas wells producing water. The data shows the production status for each well whether it is under liquid loading or not.

This set of data can be utilized to validate the proposed well-reservoir coupled model. Water production is calculated automatically, reservoir compressibility as well. The relative permeability correlation used for well 1 is shown in figure 9. The rest of the wells have the same curve coefficients as in well 1 except for the initial gas and water relative permeability.

Unfortunately, the relative permeability relationship curves for the wells in table 6 are not available. The model utilizes default relationship values that can be tuned for each reservoir. Table 7 shows the tuned initial relative permeability for both phases. The model, based on the provided values of the initial permeabilities, construct the relationship curve as in figure 9.

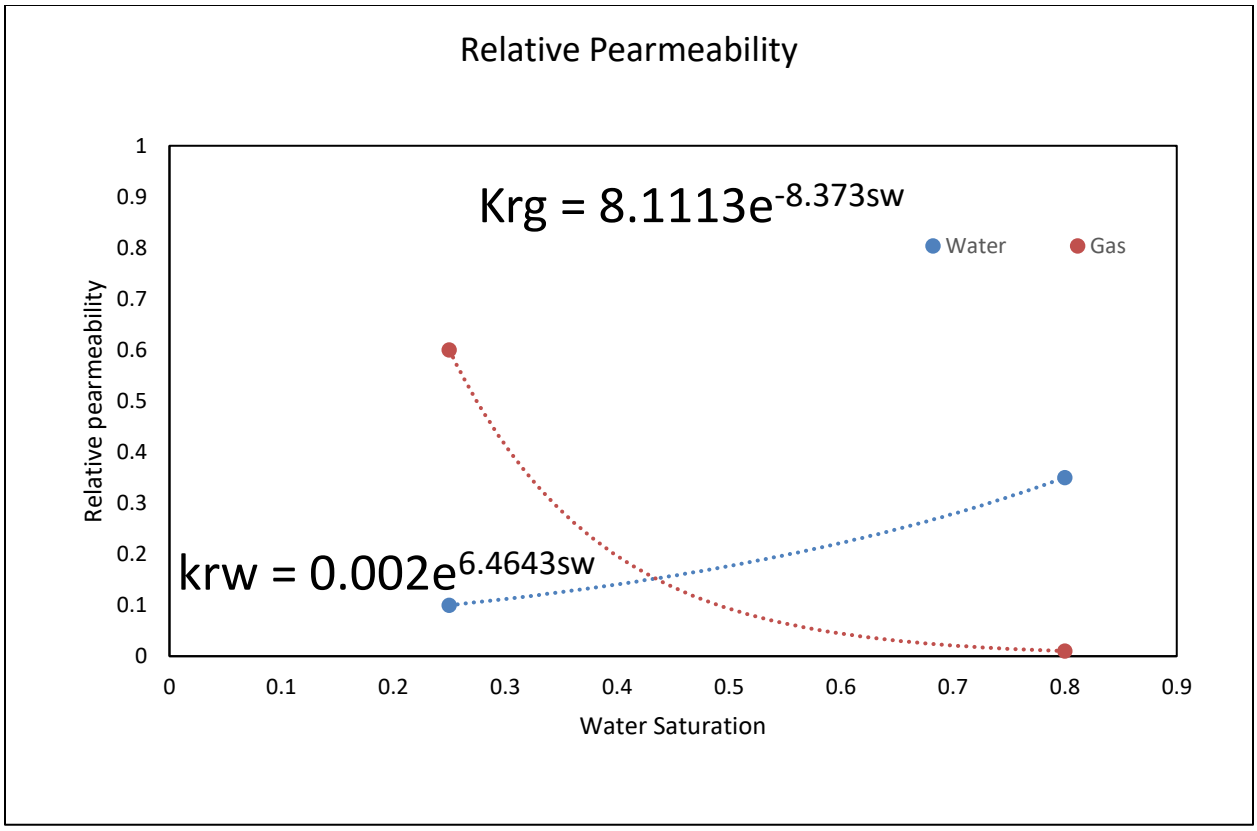

Figure 8 Relative permeability curves relationship for the validation case of the field data

Table 7 Relative permeability curve parameters for the wells listed in Table 6

Well	Initial Gas Relative Permeability	Initial Water Relative Permeability
1	0.668	0.01
2	0.668	0.01
3	0.668	0.03
4	0.668	0.019
5	0.668	0.019
6	0.668	0.03
7	0.668	0.03
8	0.133	0.03
9	0.133	0.1

Validation Against Numerical Simulation

In the literature review section, we have talked about a study done by Limpasurat and Valko et al. (2015). They created a coupled wellbore-reservoir model using an open source reservoir simulation code and Turner et al. (1969) model to predicate the onset of liquid loading. Their reservoir modeling is a sophisticated one where the whole reservoir is gridded into smaller grids. Table 8 adapts the reservoir and wellbore description from Limpasurat, et al., 2015.

Table 8 Simulation Data adapted from (Limpasurat, et al., 2015)

Reservoir Parameters	
Layer thickness	600 ft
Reservoir Radius	1,000 ft
Porosity	0.1
Permeability	1.5 md
Initial reservoir pressure	970 psi
Initial water saturation	0.3
Reservoir temperature	260 ^{o}F
Well Parameter	
Open hole diameter	7 in
Tubing diameter	5 in
Total depth	7,700 ft
Wellhead pressure	430 psi
Wellhead temperature	60 ^{o}F

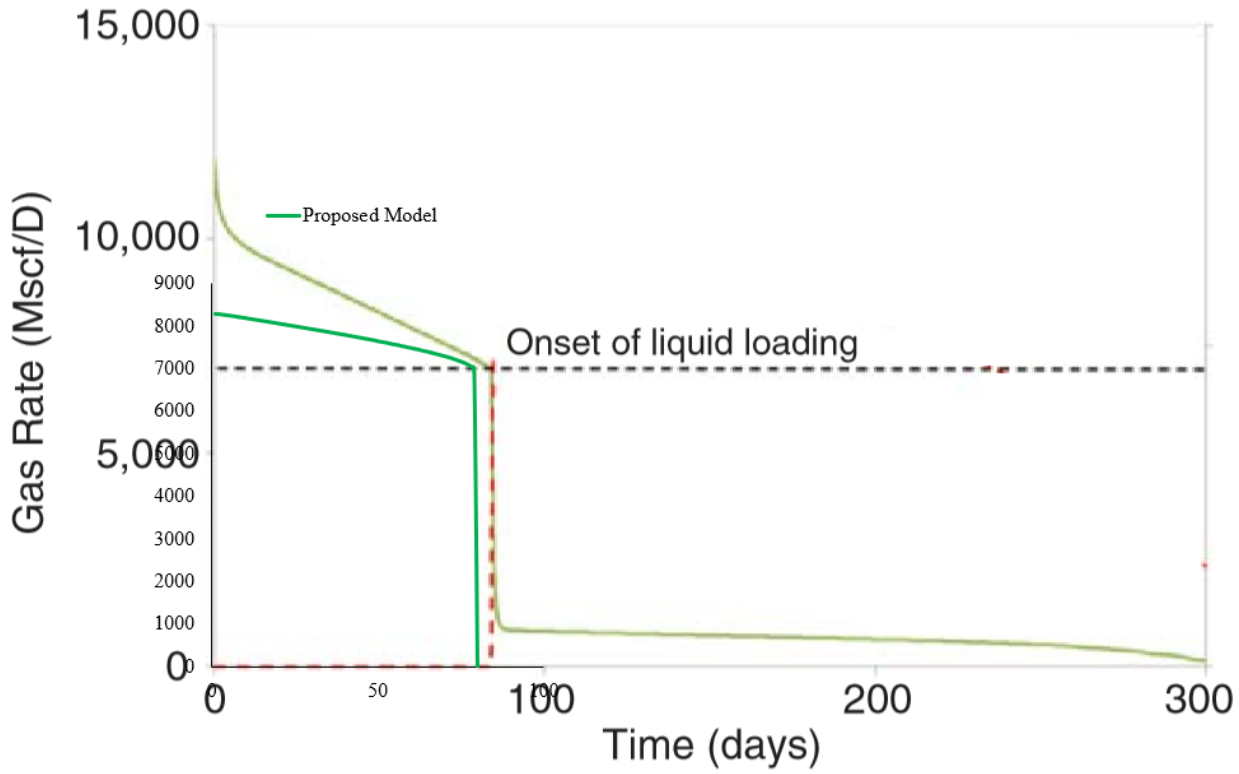

Figure 9 Comparison between open source simulation result and the proposed model

The result between our proposed model which is based on a single reservoir block is compared to the result obtained from the coupled model based on reservoir simulation are presented in Figure 10. The onset of liquid loading from our model agrees well with the time suggested by the numerical simulation. The decline of the gas flow rate is steeper in the reservoir simulation. The reason for this could be different things. Relative permeability curve equations implemented in the simulation or the correlations used to estimate fluid properties. The start of simulation production represents the ability of the simulation to take care of wellbore storage. The lower production rate after the liquid onset in the simulation is the result of water flooding job which cannot be replicated with the proposed model.

CHAPTER IV

HASAN-KABIR MODEL MODIFICATION

Hasan-Kabir pressure drop in the wellbore mechanistic model is widely used in the industry because of its simplicity. All other mechanistic models are known for their complexity and the tremendous time and efforts needed to implement them. One might argue that the other complex models might yield better accurate results, this is partially true. One should consider the percentage of improvement and the time needed to reach the final results when comparing mechanistic models. At any rate, in the model we are suggesting in this study, any model can be used. As we stated earlier, the model is built as a block algorithm where any correlation or model used can be removed and replaced by different ones that suit the user goals.

In this section, we will show that Hasan-Kabir model was developed for oil wells originally. We will prove that the transition between flow pattern is different if the gas velocity is increasing in oil well, and the gas velocity is decreasing in a gas well.

The utilization of the model proposed in this study made the investigation of Hasan-Kabir clearer. The reason is, the model is simulating a well connecting to a reservoir dynamically until the well dies. From the output, we can see snapshots of the daily flow pattern changes inside the wellbore. This closer look gives the investigator a more transparent image of what is occurring inside the wellbore.

Applying Hasan-Kabir Original Model

In this chapter a particular case is run to investigate Hasan-Kabir model, we have noticed some discontinues in the liquid holdup curves with times. These gaps occur whenever the flow

pattern changes. We found the causing of these gaps is the smoothing parameters used in Hasan-Kabir model.

Table 9 Input data used to study Hasan-Kabir model

Reservoir			Wellbore			Stream		
p_i	2,000	psia	p_{wh}	290	psia	T_{pc}	392.86	R
T	212	F	T_{wh}	129.2	F	p_{pc}	676.904	psia
A	160	acres	d	3.5	in	MW	17.382	lbm/lb mole
k	5	md	ε	6.E-03	ft	γ_g	0.6	
h	30	ft	θ	90				
ϕ	0.12	fraction	r_w	0.46	ft			
S_{wi}	0.25	fraction	Depth	5,000	ft			
ρ_w	61	lbm/ cu ft						

Table 9 shows the input data to study Hasan-Kabir model. The data presented in the table is assumed. We took into consideration a case in which the wellbore will undergo all different types of flow pattern before it dies. It is a gas reservoir which produces mainly gas at the beginning of production. The gas velocity decline shortly as initial reservoir pressure is not high enough.

To give a better glimpse of inside the wellbore, Figure 9 illustrates the changes in flow pattern at the bottom of the wellbore for different days of production. At day 83, the well produces under annular flow where the gas is flowing at the center, and the liquid is coating the wellbore pipe. As for the liquid loading, the well exhibits liquid-loading-free stage where all the liquid droplets are being transported to the surface.

At day 84, the wellbore has three different types of flow pattern. At the bottom of the well and for almost 3,000 ft, the flow is slug flow. Above the slug flow, there is churn flow for less than 1,000 ft. At the top of the wellbore, the flow pattern is annular flow.

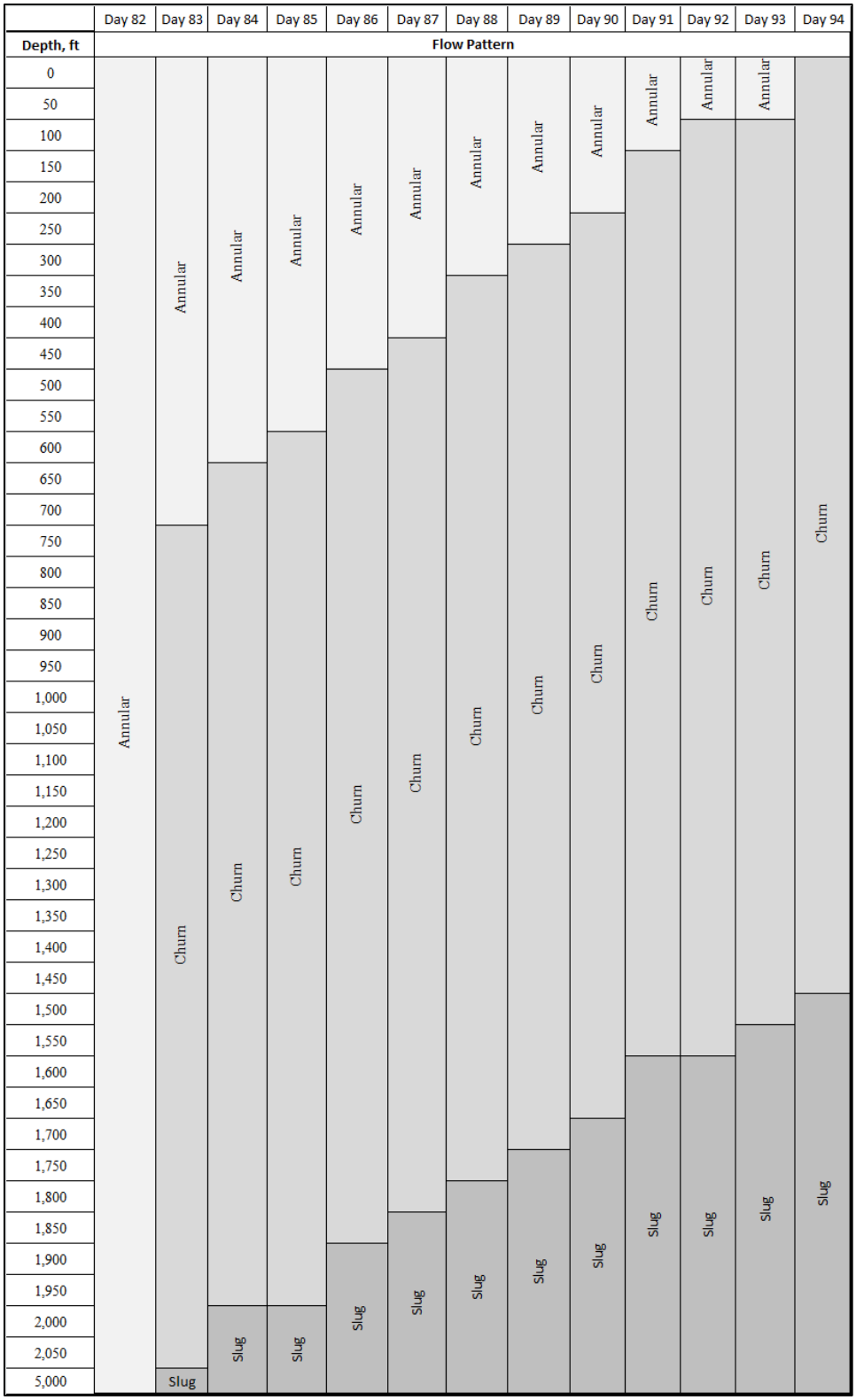

Figure 10 Flow pattern changes inside the wellbore for Hasan-Kabir Model modification case

According to Figure 11, the annular flow disappears at day 94 of production. Using wellhead conditions to detect the onset of liquid loading would result in underestimation of one week. As reservoir pressure depletes more, the wellbore will exhibit one type of flow, which is slug flow. The column of liquid under churn flow is shrinking over time.

The transition from annular into either churn or slug flow occurs first at the bottom of the well. At the bottom of the well, the pressure is higher than anywhere inside the well which means that the gas molecules are under pressure, hence, cannot move faster compared with the molecules under less pressure. In other words, the gas velocity at the bottom of the well is the lowest in the entire wellbore. Slower gas velocity is translated to the inability of gas to carry the liquid loading, which initiates the onset of liquid loading.

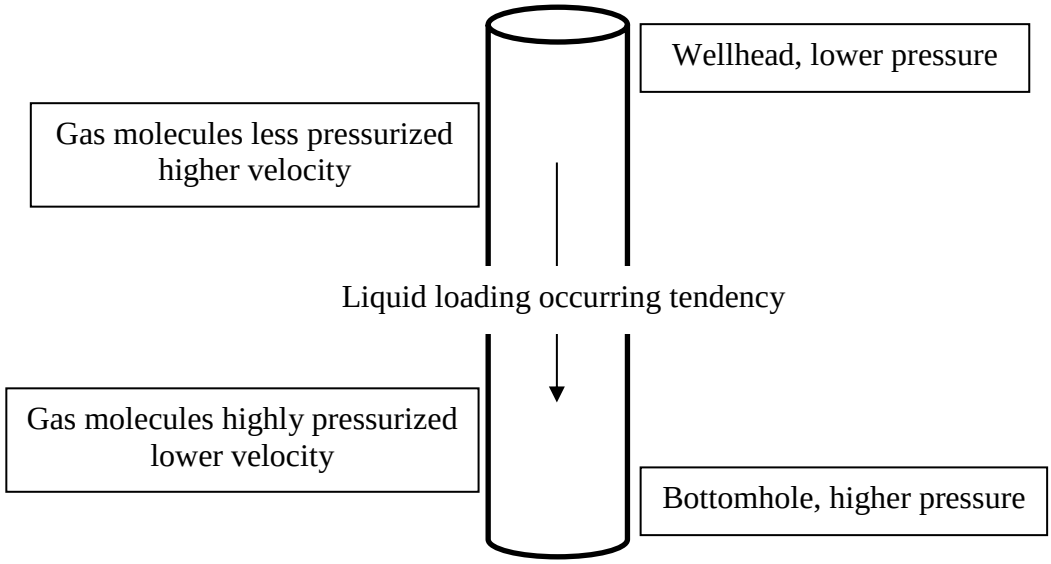

Figure 11 Illustration of liquid loading occurring tendency in wellbore

Figure 11 shows the variation of the liquid holdup in the wellbore against depth. Logically, the value of liquid holdup is higher at the bottom of the well because of the lower gas

velocity explained earlier and illustrated in Figure 12. If the gas is unable to lift the liquid, liquid drags against the pipe surface resulting in a higher liquid holdup.

Hasan-Kabir Model Shortcoming

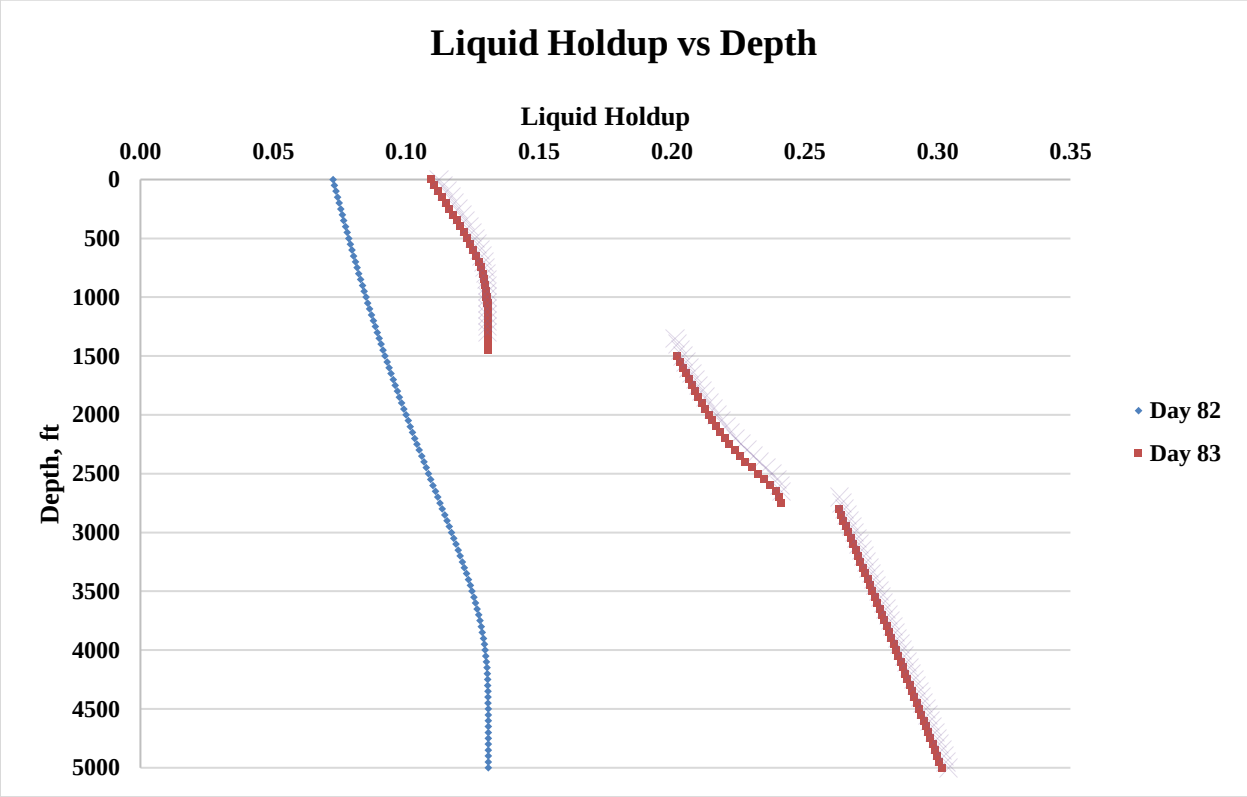

Figure 12 Liquid holdup inside the wellbore calculated with Hasan-Kabir model for two consecutive days

If we examine the curves closely in Figure 13, we can see that the entire wellbore on day 82 is under annular flow even if we do not have Figure 11 which expresses this conclusion explicitly. The reason behind the conclusion is, liquid holdup value is too small to form liquid slugs of any shape. The curve for day 83 has a gap. The liquid holdup value jumps from 0.13 to a value greater than 0.2 within a very short vertical distance which does not occur in real wells.

Figure 13 raises two questions. One, why the liquid holdup value stays almost constant at the end of annular flow pattern and before the transition into churn flow? Two, why the value of liquid holdup jumps when flow pattern changes from annular to churn flow? To be able to answer these two questions, we should recall some equations from Hasan-Kabir model.

$$f_g = \frac{v_{sg}}{c_o v_m + v_\infty} \tag{38}$$

Eq. 38 is the general equation used to calculate void fraction and liquid holdup. For annular flow, $C_o = 1$ and v_∞ is 0.

$$f_g = \frac{v_{sg}}{v_{sg} + v_{sl}} \tag{50}$$

Assume, the liquid velocity is constant, and the gas velocity decreases from a high value which is the same situation in any gas wellbore. The liquid velocity does not change that much as liquid is slightly incompressible which means, it cannot vary a lot with the pressure changing. The following table represents the results for this assumption. Since the liquid velocity is minimal compared to gas velocity in annular flow:

$$f_g = \frac{v_{sg}}{v_{sg} + C} \approx 1 \tag{51}$$

At the top of the wellbore, gas velocity changes with depth considerable as gas molecules are not under high pressure. However, at the bottom of the, when the pressure is high, gas velocity cannot change significantly with depth, resulting in an almost constant liquid holdup which explains the constant part of the day 82 curve below 4,000 ft, and the top part of curve day 83 as gas velocity low enough to change the flow pattern into churn flow Figure 11.

As for the discontinuity observed in day 83 curve, it occurs as flow transitions into churn flow from annular which occurs gradually in reality. In Figure 11, the liquid holdup jumps from 0.13 to 0.23 instantaneously. Let's recall churn flow void fraction equation.

$$f_g = \frac{v_{sg}}{c_o v_m + v_\infty} \tag{38}$$

The value of liquid holdup before the flow goes into the churn flow is around 0.13. The reason behind this is the flow parameter C_o in Hasan-Kabir model. For a high gas velocity in the churn flow equation as liquid velocity becomes insignificant, the equation turns to:

$$f_g = \frac{v_{sg}}{1.15 v_{sg}} \approx 0.87 \tag{52}$$

This results in a liquid holdup value of

$$f_l = 1 - f_g = 1 - 0.87 = 0.13 \tag{53}$$

For churn flow, C_o is 1.15, and the rise velocity is a value around 1.1. Comparing this equation to the annular flow equation (Figure 14), we notice an addition to the dominator in the form of a constant and the rise velocity. In other words, C_o suddenly changes from 1 to 1.15 and the rise velocity increases from zero to nearly 1.1. This is the main reason for the jump.

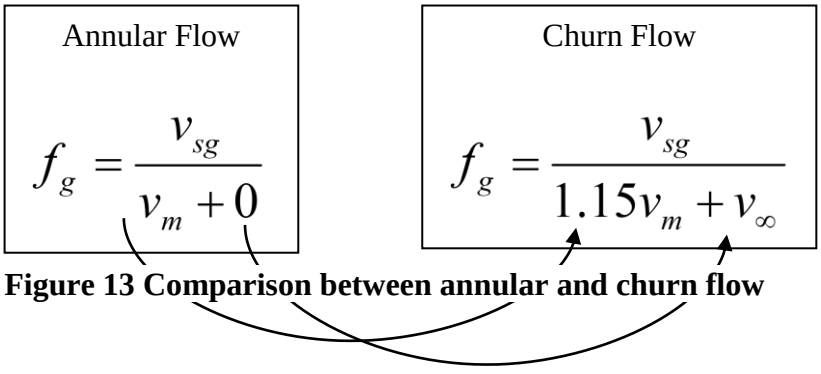

Figure 13 Comparison between annular and churn flow

Hasan-Kabir Model Improvements

Hasan-Kabir tried to solve this issue by adding a smoothing parameter to the annular flow equation to aid in bridging the gap by having a variable Co starts with a value of 1 and goes up to a value of 1.15, which is the Co for churn flow.

$$c_o = 1.15\left(1-\exp\left(-0.1\frac{v_{gc}}{v_{sg}-v_{gc}}\right)\right)+\exp\left(-0.1\frac{v_{gc}}{v_{sg}-v_{gc}}\right)$$

The smoothing parameter consists of two similar terms. To be able to understand this equation, Table 10 shows the tabulated results for the smoothing parameter for arbitrary value of 10 for annular critical velocity.

Table 10 Hasan-Kabir annular flow smoothing parameter terms at different gas velocities

v_{sg}	$1-\exp\left(-0.1\frac{v_{gc}}{v_{sg}-v_{gc}}\right)$	$\exp\left(-0.1\frac{v_{gc}}{v_{sg}-v_{gc}}\right)$
20	0.095	0.90
19	0.11	0.89
18	0.12	0.88
17	0.13	0.87
16	0.15	0.85
15	0.18	0.82
14	0.22	0.79
13	0.28	0.72
12	0.39	0.61
11	0.63	0.37

The smoothing equation is a function of superficial gas velocity and the critical annular velocity. The equation consists of two terms adding them equals one for any gas velocity. Also, one term goes from small number near zero up to one. The other term decreases from a value near one to zero. Multiplying the left-hand side term with a value of 1.15 results a number near 1

and goes up to reach the same multiplier value 1.15. It is an exponential equation results values from 1 to 1.15

When Hasan-Kabir modified their original work, they worked only on the constant parameter in their general equation to calculate the void fraction. This improvement resulted in smoother void fraction and liquid holdup curves. However, the improvements do not affect the presented case where we still have a gap or discontinuity in the liquid holdup curve. Looking at Figure 11, Hasan-Kabir wanted to have a smooth transition from a flow pattern to other which works perfectly for all other flow transitions but not for the transition to the annular flow. It seems that Hasan-Kabir has been developed to work for two-phase flow with liquid is the dominated phase. As gas velocity increases, flow pattern changes from bubbly to churn or slug flow during these transitions, Hasan-Kabir works fine up until it reaches annular flow. Since we are investigating liquid holdup, which occurs as flow transits from annular, it is essential to have an accurate annular transition equation as possible. As a result, bubble rise velocity in the annular flow equation should be modified.

We need an exponential equation for the bubble rise velocity gives values near zero at high gas velocity and values near the bubble rise velocity values for churn flow at lower gas velocity. The equation should be a function of superficial gas velocity and the critical gas velocity to have an annular flow. We will start with Eq 33 as a base equation.

$$v_{\infty AC} = \left(1 - \exp\left(-0.1\frac{v_{gc}}{v_{sg} - v_{gc}}\right)\right) + \exp\left(-0.1\frac{v_{gc}}{v_{sg} - v_{gc}}\right) \qquad 33$$

As can be seen from Table 10, the left-hand side term of the equation results in small values (near zero) at high gas velocity and higher values at higher gas velocities. Eliminating the right-hand side term results in Eq 54.

$$v_{\infty AC} = 1 - \exp\left(-0.1 \frac{v_{gc}}{v_{sg} - v_{gc}} \right) \quad 54$$

To make sure we are heading in the right direction, we will present the original values for the rise velocity for a specific day and see how they change with flow pattern.

Table 11 Data from day 86

Depth	Flow Pattern	v_∞	C_o
450	Annular	0	1.1500
500	Churn	1.063	1.1632

Table 11 shows the values of rise velocity with depth. For annular flow, they are all zeros, but for churn flow, they start with a value of 1.063 and decreases afterward. As for C_o values, they have a reasonable transition from annular to churn flow, but it can be enhanced further. First, we will use Eq. 54 to produce rise bubble velocity for annular flow.

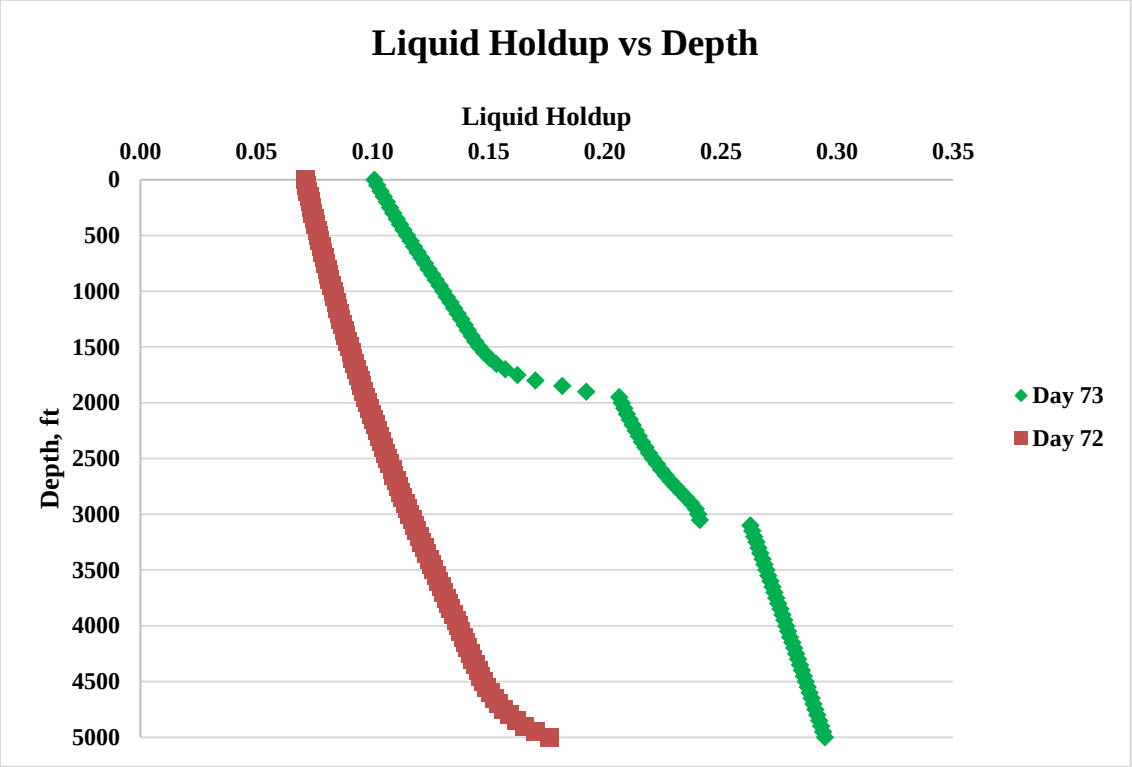

Figure 14 Modified Hasan-Kabir model Liquid holdup vs. Depth

As can be seen from Figure 15, the curve shape has improved a lot. At day 72 when the flow pattern is annular throughout the entire wellbore, the liquid holdup values do not stay constant at the bottom of the wellbore. They start to shift toward churn flow curve. At day 73, flow pattern changes at 1750 ft. The transition is smoother compared to Figure 13. The transition from churn to slug needs smoothing. Liquid loading onset occurs ten days earlier than the original model which is due to adding bubble rise velocity to the dominator of the void fraction equation, which makes void fraction smaller and liquid holdup larger.

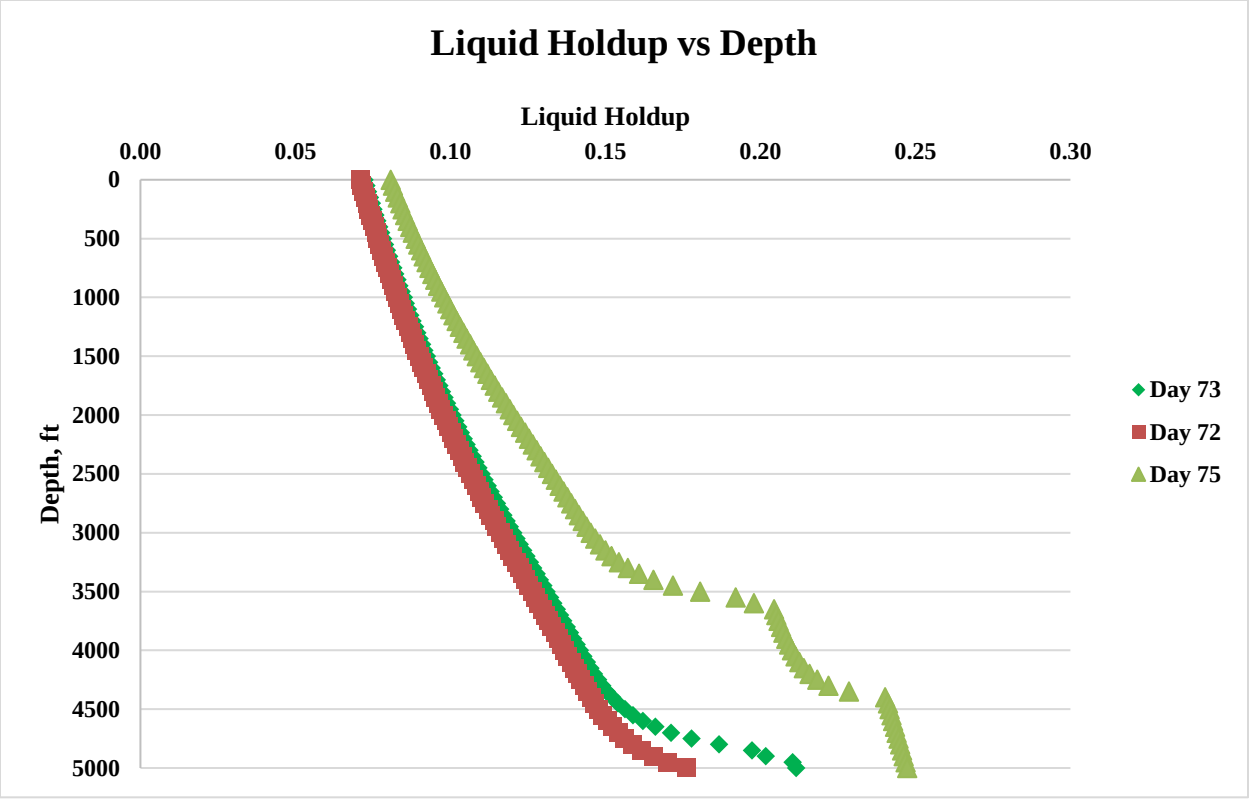

Figure 15 Final modified Hasan-Kabir model result for liquid holdup vs. depth

Figure 16 shows the improved results from Hasan-Kabir. The transition from a flow pattern into other flow pattern is much smoother. The reason behind the small jumps in liquid holdup values is the smoothing equation. The equation has an exponential expression where the exponent controls how fast or slow the values increase. In the original work of Hasan Kabir, the exponent has a value of -0.1. In the enchanted version, -0.02 seems to give better results. We need to bridge the gap between the annular and the churn flow. As a result, the rise velocity should increase from zero up to a value near the first value of the rise velocity for the churn flow. If we increase the value to one rapidly, this will have a significant impact on the prediction of liquid loading onset because increasing the rise velocity will increase the liquid holdup. Ideally,

at high gas velocity rise velocity for annular flow should be near zero, and at lower gas velocity, it should be near 1.Table 12 summarizes the modification to Hasan-Kabir.

Hasan-Kabir Model Improvements Summary

Table 12 Hasan-Kabir model improvements summary

Flow Parameter, C_o		
Annular Flow	Original Model	$c_o = 1.15\left(1-\exp\left(-0.1\frac{v_{gc}}{v_{sg}-v_{gc}}\right)\right)+\exp\left(-0.1\frac{v_{gc}}{v_{sg}-v_{gc}}\right)$
	Modified Model	$c_o = 1.15\left(1-\exp\left(-0.2\frac{v_{gc}}{v_{sg}-v_{gc}}\right)\right)+\exp\left(-0.2\frac{v_{gc}}{v_{sg}-v_{gc}}\right)$
Churn Flow	Original Model	$C_o = 1.15\left[e^{-0.1v_{ms}/(v_{sg}-v_{ms})}\right]+1.2\left[1-e^{-0.1v_{ms}/(v_{sg}-v_{ms})}\right]$
	Modified Model	$C_o = 1.15\left[e^{-0.01v_{ms}/(v_{sg}-v_{ms})}\right]+1.2\left[1-e^{-0.01v_{ms}/(v_{sg}-v_{ms})}\right]$
Rise Velocity		
Annular Flow	Original Model	$v_\infty = 0$
	Modified Model	$v_{\infty AC} = 1-\exp\left(-0.01\frac{v_{gc}}{v_{sg}-v_{gc}}\right)$

CHAPTER V

RESERVOIR PRESSURE AND LIQUID LOADING

Reservoir Initial Pressure Effect on Liquid Loading

The reservoir is the main factor affecting liquid loading phenomena. The reservoir is not only responsible for liquid loading; it is the primary source of everything in petroleum engineering. Going away from the wellbore and the many correlations developed to study the phenomena of liquid loading, in this section, the effect of the reservoir will be examined thoroughly. We will start with reservoir pressure. Reservoir pressure is the engineering term for reservoir energy. When the reservoir energetic, high pressure, flowrate is high, and production is high which occurs at the early stages of production. As time progress, the reservoir starts to deplete. How depletion affect liquid loading? This is the central question we want to find an answer to it. Of course, liquid loading onset occurs at a later stage when initial reservoir pressure is high. In other words, the higher reservoir pressure, the better. However, for how long? Does it make any difference if the reservoir pressure can be increased 100 psi? For the reservoir and wellbore properties shown in Table 13, we plotted different reservoir pressure flow rates against time as shown in Figure 15.

Table 13 Reservoir and wellbore properties data used in our model for this section

Reservoir			Wellbore		
p_i	3,200	psia			
T	212	F	p_{wh}	290	psia
A	160	acres	T_{wh}	129.2	F
k	5	md	d	3.5	in
h	30	ft	ε	6.E-03	ft
φ	0.12	fraction	θ	90	
S_{wi}	0.25	fraction	r_w	0.46	ft
ρ_w	61	lbm/ cu ft	Depth	5,000	ft

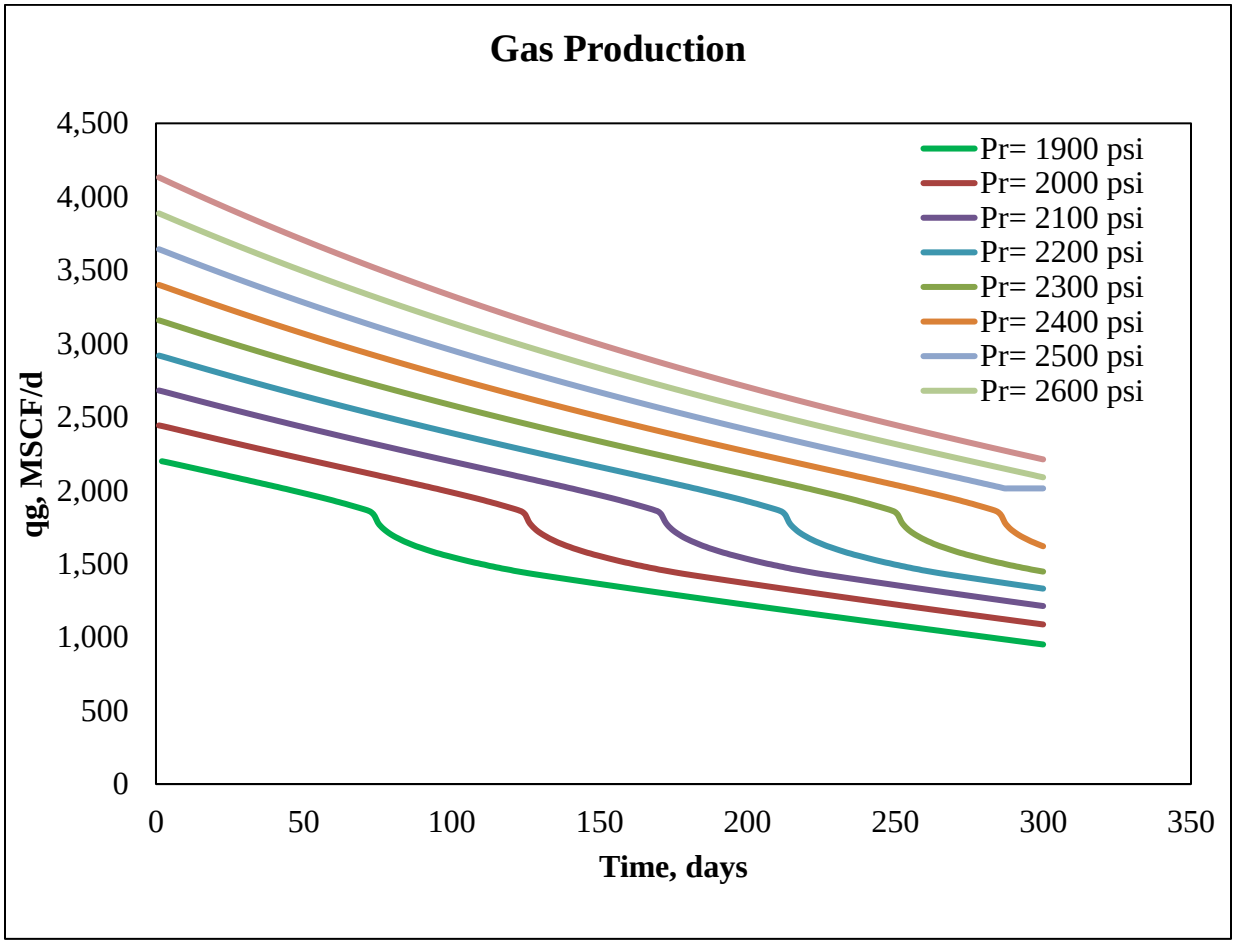

Figure 16 Gas production for the same reservoir for different initial reservoir pressure

Figure 15 presents gas flow rate vs. time for different initial reservoir pressures. Initial reservoir pressure starts in this plot at 1900 psi and increases to 2700 psi. Each time initial reservoir pressure increases, liquid loading onset occurs at a later time.

Liquid loading onset can be detected from the curves as the shape of the curves shift. The shift of the shape is the result of flow pattern shifting as well. However, from the plot itself, we cannot know if it shifts to slug or to churn flow.

The interesting finding from this plot is the gap between liquid loading onset decreases as reservoir pressure increases. It is true that the higher the reservoir pressure is, the later the liquid loading onset will occur. However, as reservoir pressure increases, the liquid loading onset gap is delayed for a shorter and shorter time. Liquid loading onset time is reported in Table 14.

Table 14 Tabulated results for Figure 15

Reservoir Pressure, psi	Liquid Loading Onset, day	Δ Time, days	Flow Pattern changes from annular to
1900	73		Churn
2000	124	51	Churn
2100	171	47	Churn
2200	212	41	Churn
2300	250	38	Churn
2400	285	35	Churn
2500	288	3	slug

From Table 14, we can see that liquid loading starts at 51 days later as initial reservoir pressure increased 100 psi. One might expect that it would occur at later 50 days if reservoir pressure is increased another 100 psi. However, it does not. On the contrary, if reservoir pressure increased 1000 psi, liquid loading onset occurs after 47 days. The gaps get shorter as the reservoir initial pressure increases until it becomes only three days.

Reservoir Pressure and Wellbore Flow Pattern Relationship

The reason behind this is a rather complicated matter. It cannot be guessed from Table 14. The good thing about the proposed model is that it gives pages of outputs detailing daily production. Table 15 is an example of the data that can be acquired from the model.

Table 15 Further production data for the same well under different initial reservoir pressures

Time	p_r	p_{wf}	q_g	q_w	FP	f_L
days	psi	psi	MSCF/d	STB/d		
P_{ri}=	1900	psi				
72	1,779	585	1,860	5	Annular	0.176
73	1,777	597	1,848	5	Churn	0.212
74	1,776	622	1,824	5	Slug	0.241
P_{ri}=	2,000	psi				
123	1,779	584	1,862	5	Annular	0.172
124	1,778	592	1,852	5	Churn	0.210
125	1,776	614	1,832	5	Churn	0.223
126	1,775	662	1,788	5	Slug	0.246
P_{ri}=	2,100	psi				
170	1,778	590	1,854	5	Annular	0.201
171	1,776	613	1,833	5	Churn	0.221
172	1,775	657	1,793	5	Slug	0.246
P_{ri}=	2,200	psi				
211	1,779	585	1,861	5	Annular	0.174
212	1,777	594	1,850	5	Churn	0.211
213	1,776	619	1,828	5	Churn	0.232
214	1,774	665	1,785	5	Slug	0.247
P_{ri}=	2,300	psi				
249	1,779	584	1,861	5	Annular	0.172
250	1,778	593	1,852	5	Churn	0.210
251	1,776	616	1,830	5	Churn	0.226
252	1,775	662	1,788	5	Slug	0.246
P_{ri}=	2,400	psi				
284	1,779	585	1,860	5	Annular	0.176
285	1,777	596	1,848	5	Churn	0.211
286	1,776	622	1,824	5	Slug	0.241
P_{ri}=	2,500	psi				
287	1,826	512	2,014	6	Annular	0.098
288	1,824	852	2,014	6	Slug	0.284

From Table 15, further information about the situation is available. The table shows the time in days. This time represents the number of daily production. For example, 72 days means the 72nd day after the first day of production. The table displays flowrates for both fluids for that specific day. We can see the flow pattern at the bottom of the well on that day. This flow pattern represents the bottom only; it does not mean that the entire wellbore is under this flow. The table shows the flow pattern at the bottom only because the bottom part of the wellbore is the first location where liquid loading onset occurs which is enough to give us an image of what is going inside the wellbore. Lastly, the liquid holdup is displayed.

At initial reservoir pressure of 1900 psi, flow pattern changes from annular to churn flow. The next day it changes into slug flow. Churn flow does not disappear entirely from the wellbore. It just travels upward. In other words, churn flow seems like the transition between annular flow and slug flow.

At initial reservoir pressure of 2000 psi, flow pattern changes into churn flow and stays at churn flow for one more day until it shifts again into slug flow. In other words, the transition from annular into slug flow took a longer time. It behaves the same way for initial reservoir pressures of 2100, 2200, 2300, and 2400 psi.

From table 15, we notice that at the initial reservoir pressure of 2500 psi, liquid loading onset time is only three days later than if the initial reservoir pressure is less by 100 psi. If the management were in the place of thinking to increase reservoir pressure by gas injection or water flooding to keep the reservoir pressure higher by 100 psi to avoid liquid loading, unfortunately, it would be economically unreasonable if the case as the one discussed here. The question is, why!

To look further into this matter, we have increased the initial reservoir pressure and run the simulations to see what happens. The results are tabulated in Table 16.

Table 16 Increasing initial reservoir pressure effect

Initial Reservoir Pressure, psi	Liquid Loading Onset, day	Δ Time, days	Flow Pattern changes from annular to
1900	73		Churn
2000	124	51	Churn
2100	171	47	Churn
2200	212	41	Churn
2300	250	38	Churn
2400	285	35	Churn
2500	288	3	slug
2600	348	60	churn
2700	374	26	churn
2800	399	25	churn
2900	422	23	Churn
3000	444	22	Churn
3100	464	20	Churn
3200	483	19	Churn

From table 16, it is evident that liquid loading onset "reset" at a specific value of initial reservoir pressure. Our explanation is, the length of the annular flow period is significant to the start of liquid loading. The more the flow stays at annular flow, the flow pattern tends to shift to slug flow skipping churn flow. If it stays longer, it can die without going through any change of flow pattern as the case discussed in the validation section. How long the well remains in annular flow depends on the initial reservoir pressure. However, increasing initial reservoir pressure to avoid the liquid loading onset can aid in delaying the phenomena, but it should be studied carefully. At initial reservoir pressure of 2400 psi, the flow pattern does not change into churn flow. As a result, it goes directly into slug flow. The slug flow increases liquid holdup severely

which leads to faster liquid loading onset making the increment of initial reservoir pressure meaningless. The liquid holdup for the different initial reservoir pressures is plotted against time To get a better look at this issue,

Reservoir Pressure and Wellbore Liquid Holdup Relationship

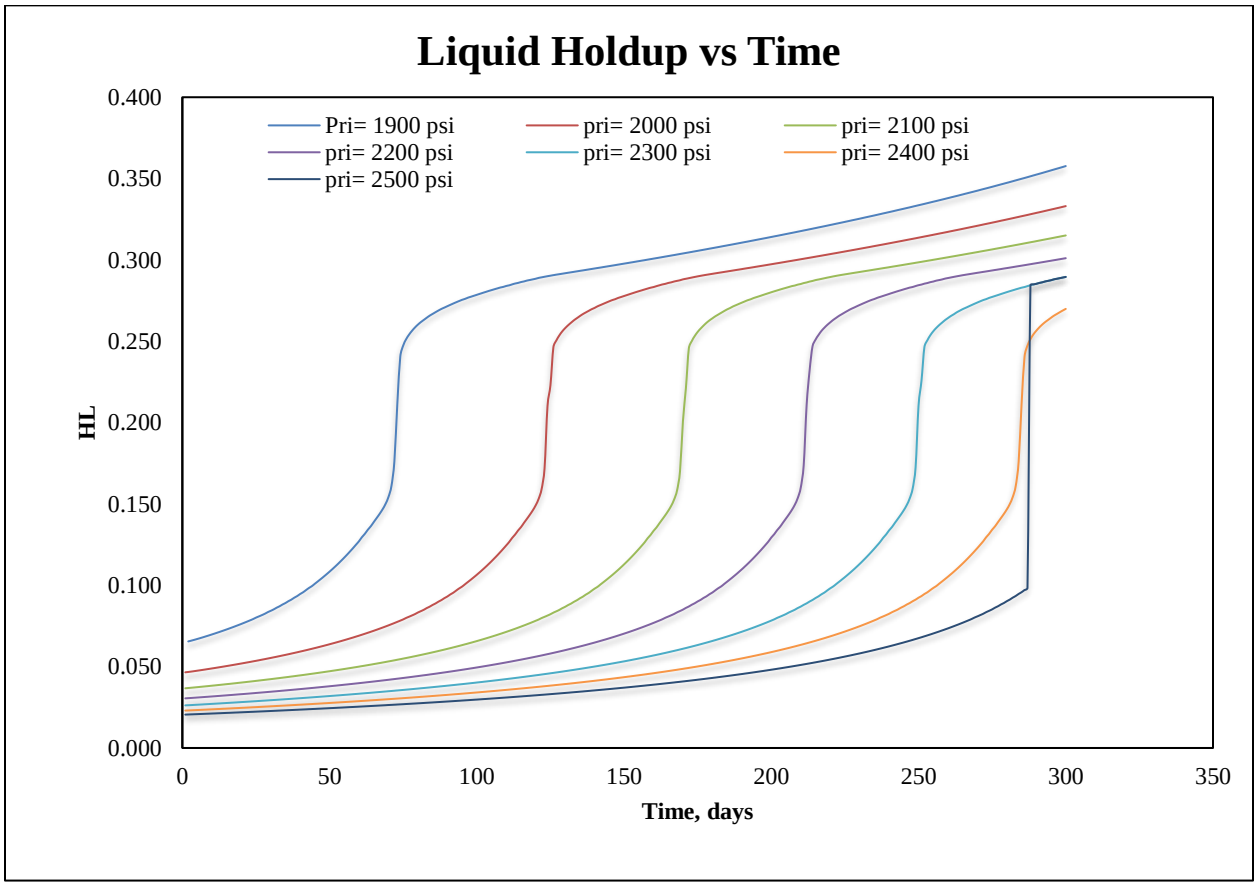

Figure 17 Liquid holdup for different initial reservoir pressure

The liquid holdup is the fraction of liquid occupying a section of the wellbore. When flow pattern is annular, the liquid holdup is the lowest compared to churn, slug, and bubbly flow. To give a general idea about liquid holdup varying with flow pattern changing, Figure 18 displays liquid holdup at the bottom of the well over time.

Table 17 Liquid holdup for different flow patterns

Liquid Holdup	Flow Pattern
0.01~ 0.15	Annular
0.15 ~ 0.25	Churn
0.25 ~ 0.8	Slug
0.8 ~ 0.99	Bubbly

Calculating the liquid holdup is still one of the most challenging issues in the two-phase flow. Typical liquid holdup values for the different flow patterns are shown in Table 17 In gas wells, annular two-phase flow dominates the early time of production, and later it changes to slug flow. Churn flow is acting as a transition phase between the annular and slug flow. It is evident from Figure 18 that the transition phase which is the churn flow pattern period is related to annular flow period. The more the well is under annular flow, the less it will be in churn flow.

To get the complete picture, reservoir pressure and bottomhole pressure for the different initial reservoir pressures studied in this section are presented here.

Bottomhole Pressure and Liquid Build up Relationship as Reservoir Depletes

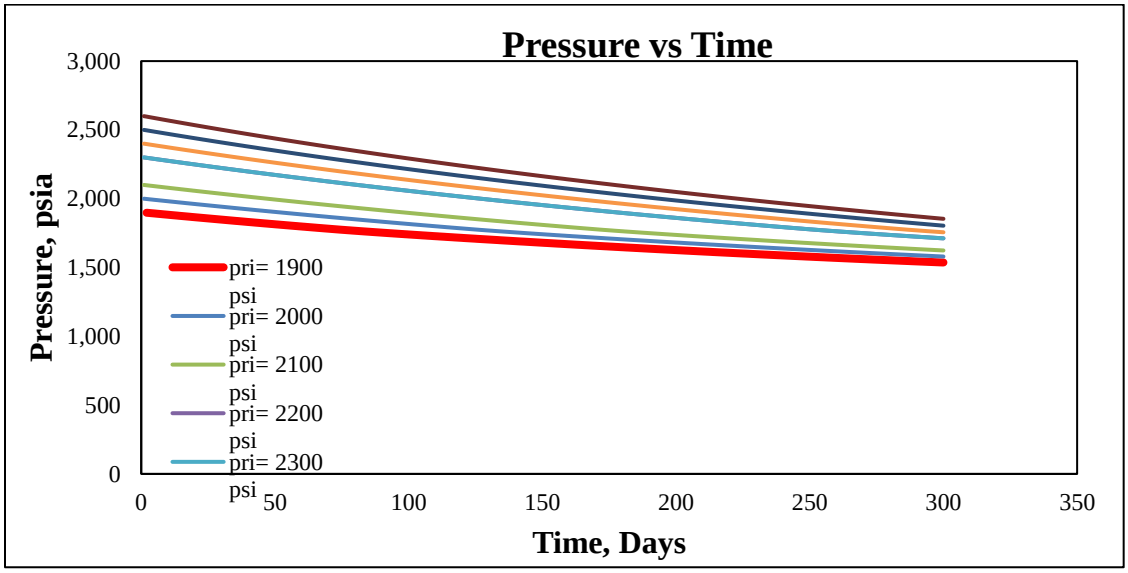

Figure 18 Reservoir pressure depletion vs. time for different initial reservoir pressure

Figure 19 shows reservoir pressure depletion over time. We can conclude from this figure that reservoir depletion is not affected by liquid loading or the two-phase flow inside the wellbore. Reservoir pressure calculated in this model does not depend on any wellbore parameter except for the daily gas production. It is determined through gas reservoir material balance which of course independent of the liquid holdup in the wellbore.

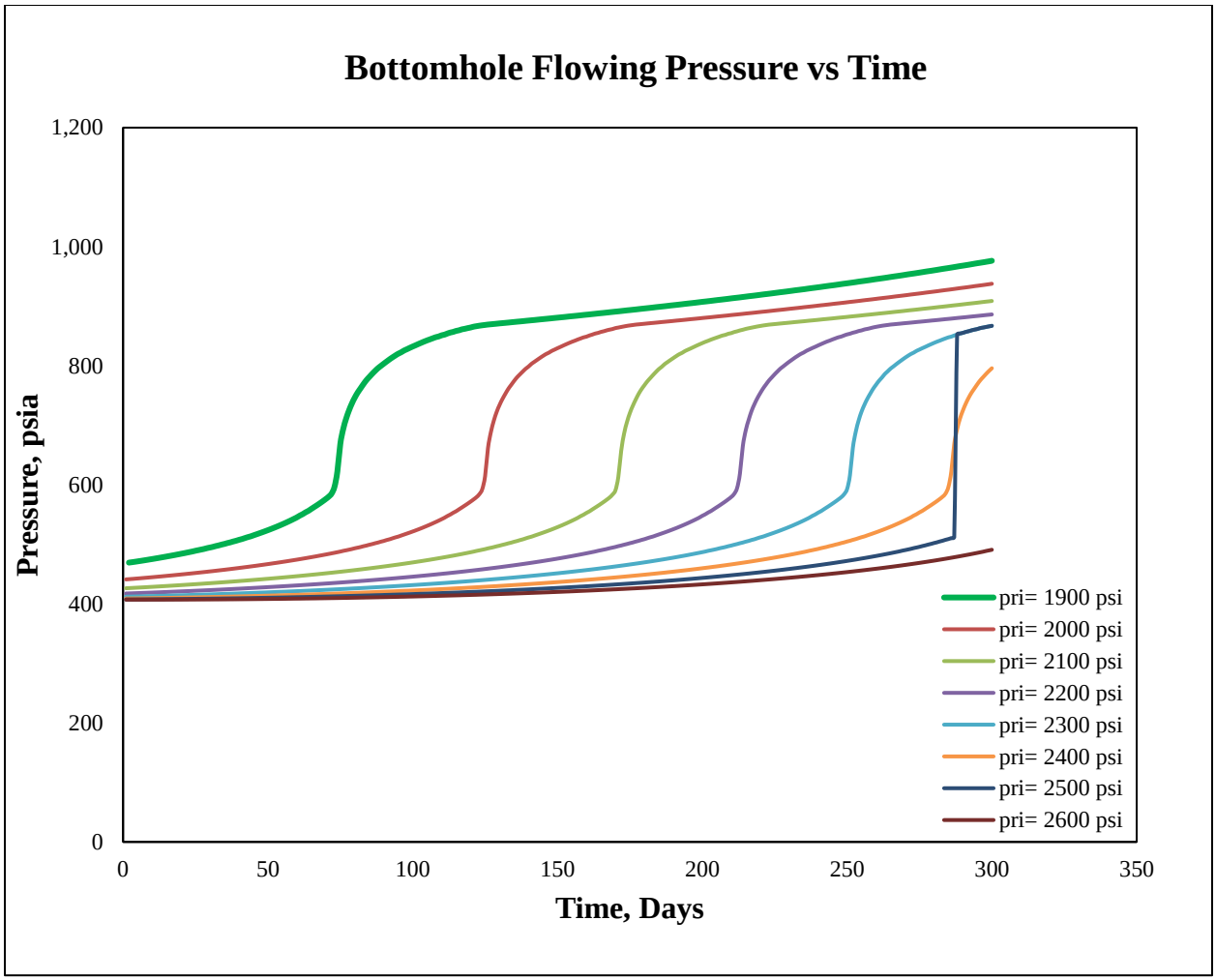

Figure 19 Bottomhole pressure for the same reservoir assuming different initial reservoir pressure

Bottomhole pressure can be affected directly by liquid loading. As liquid holdup increases inside the entire wellbore, the dense liquid content builds up causing back pressure on the bottomhole causing a sudden increase in the bottomhole flowing pressure and can be used as a sign of liquid loading onset.

Figure 20 displays how bottomhole pressure changes because of flow pattern change in the wellbore. In gas wells, bottomhole pressure increases with time as liquid condenses throughout production. The rate at which bottomhole pressure increases depends on the liquid

content in the stream. The sudden increases in bottomhole pressure in Figure 18 is due to the change of flow pattern from the annular flow. This sudden surge can be associated with churn or slug flow. However, with a closer look at the different curves representing different initial reservoir pressure, all the curves behave the same way, except for the curve belongs to the initial reservoir pressure of 2500 psi.

All the curves in Figure 18 start with a curve concave up and then concave down. After that, becomes almost a straight-line increasing with time, except for the last curve belongs to 2500 psi. It starts with a curve concaving, then suddenly shifts to a straight line. From Table 17, we can see that at the initial reservoir pressure of 2500 psi, the flow pattern changes after the onset of liquid loading from annular flow to slug flow. This behavior signifies our finding that churn flow is the transition between annular and slug flow.

Figure 18 shows the curve for initial reservoir pressure of 2600. This curve does not change. In other words, the well does not undergo any change in the flow pattern. Hence, liquid loading does not take place before the 300 days of production as the other wells. What we can understand from this behavior is, initial reservoir pressure can affect the onset of liquid loading. The same figure is plotted again, but this time showing the rest of the 2600 psi curve.

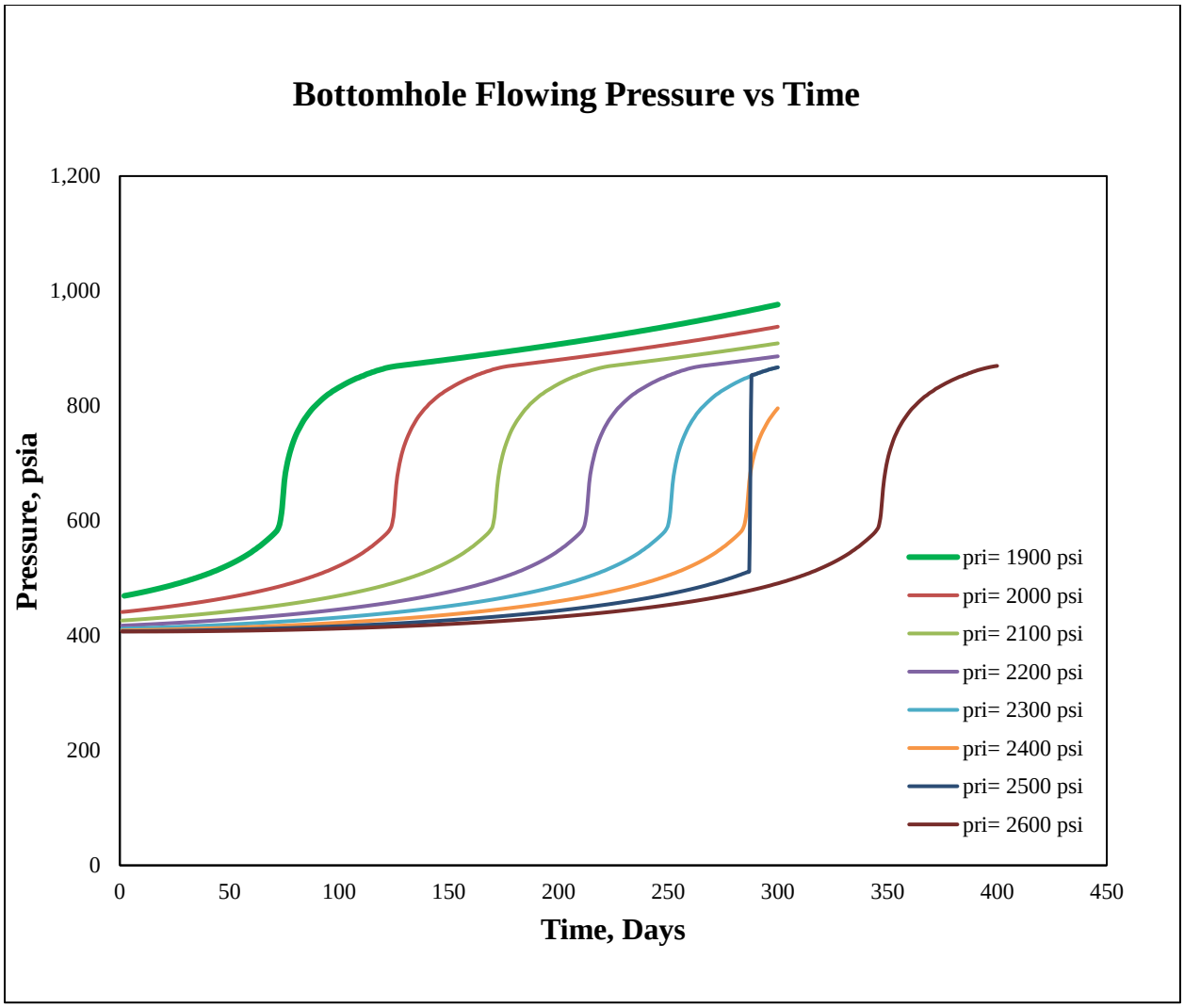

Figure 20 Bottomhole pressure at higher initial reservoir pressure

Coupling reservoir model and wellbore model allowed us to understand the effect of the reservoir on liquid loading. Figure 21 shows that the bottomhole pressure curve concaves up after the onset of liquid loading indicating that the flow patterns shift from annular to churn flow, not slug flow. This behavior confirms that the initial reservoir pressure affects the change of flow pattern. The longer the annular flow rate stays in the wellbore, the higher the possibility that it will change to slug flow directly. However, at higher intimal reservoir pressure, the wellbore can stay longer in the annular two-phase flow and changes into churn flow.

CHAPTER VI

RESULTS, DISCUSSION, AND CONCLUSION

Water Production Effect on Liquid Loading

Having easy to modify model can help with the studying of many vital parameters like the production of and its effect on liquid loading. The proposed model in this study utilizes the relative permeability concept to compute the two-phase flow in the reservoir. In this section, the effect of relative permeability and water production on liquid loading will be tackled.

Modified Brooks and Corey model (1966)

$$k_{rw} = \left(\frac{s_w - s_{wr}}{1 - s_{wi}} \right)^n \qquad 14$$

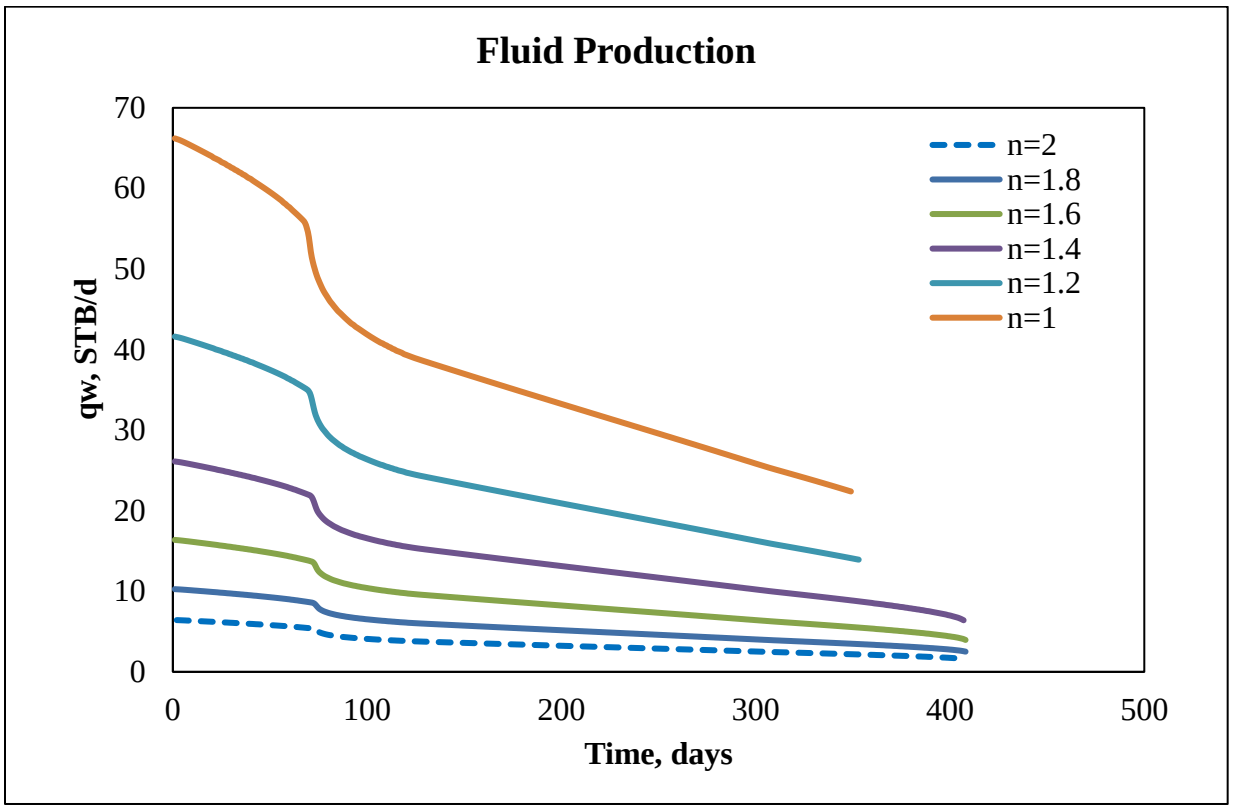

Figure 21 Water production for different reservoirs having different Corey exponent

Water flow rate for different reservoirs having different relative permeability values is plotted in Figure 22. It seems that water production does not affect the onset of liquid loading because at the early stages of production gas flow rate is very high and able to lift all the liquid to the surface regardless of the water content. Something else is worth mentioning. Water production, when the initial water production is high, decreases a lot after the onset of liquid loading. In other words, the higher is the initial water flow rate, the more it decreases after the onset of liquid loading. Now how this affects the gas flow rate?

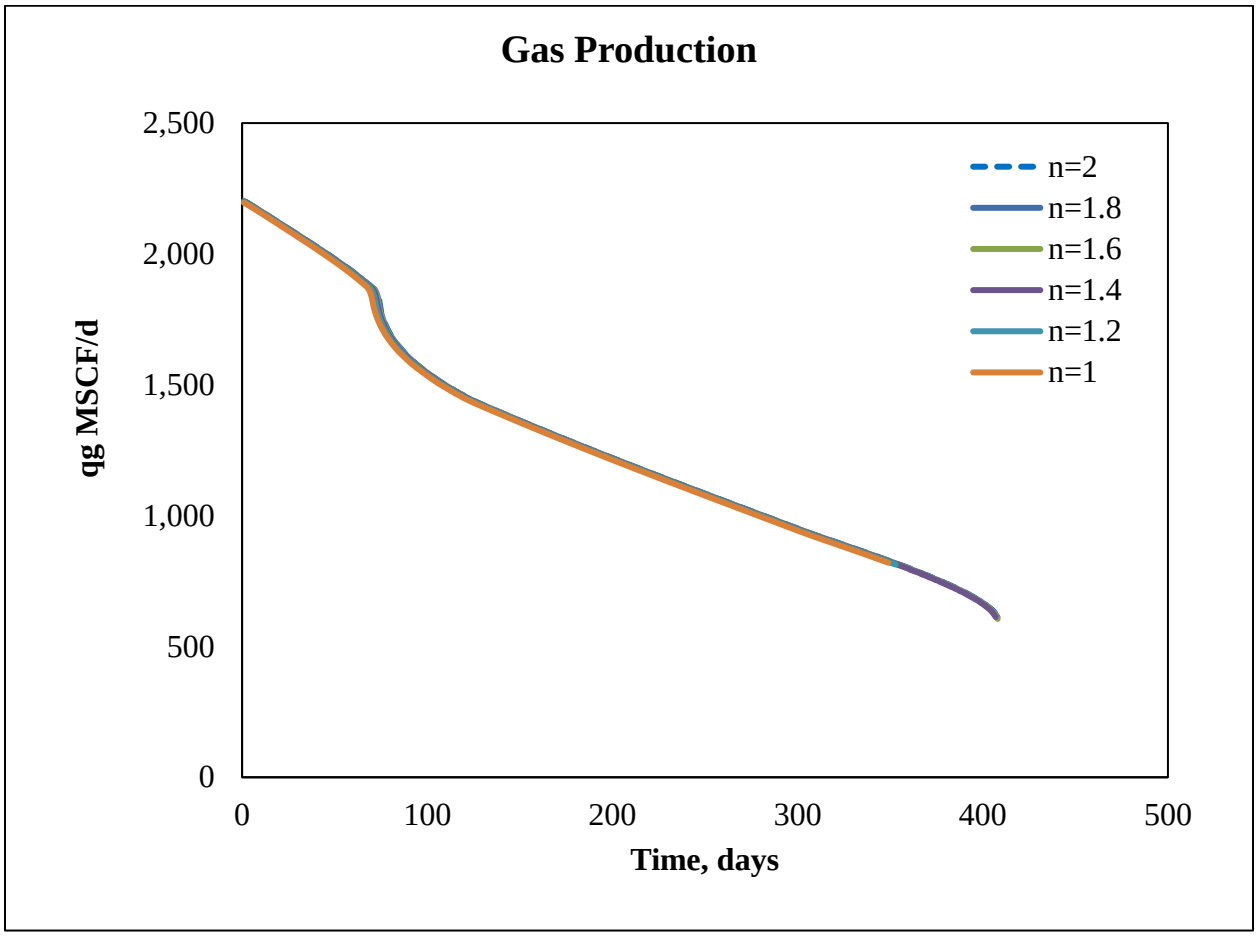

Figure 22 The effect of water production on the gas flow rate

Gas production if the flow rate is very high, going into liquid loading can be difficult. As a result, we can see from Figure 23; increasing water production did not affect the onset time of liquid loading. However, one might argue that the increment of water is still low. This might be true. In the next figure, we will try to increase water production furthermore. Before we go into that step, there is one effect we observed from increasing water production. The life of the well has decreased significantly after each increment which cannot be seen clearly in Figure 22. It is more explicit in Figure 23. When water production increases, the well-life expectancy decreases because the water content in the well increased. It is true that the onset of liquid loading time does not change. However, being in the slug flow with more water connate, this increases hydrostatic pressure drop. In other words, gas velocity is that main factor for the onset of liquid loading, and the water flow rate is the main factor affecting well life expectancy.

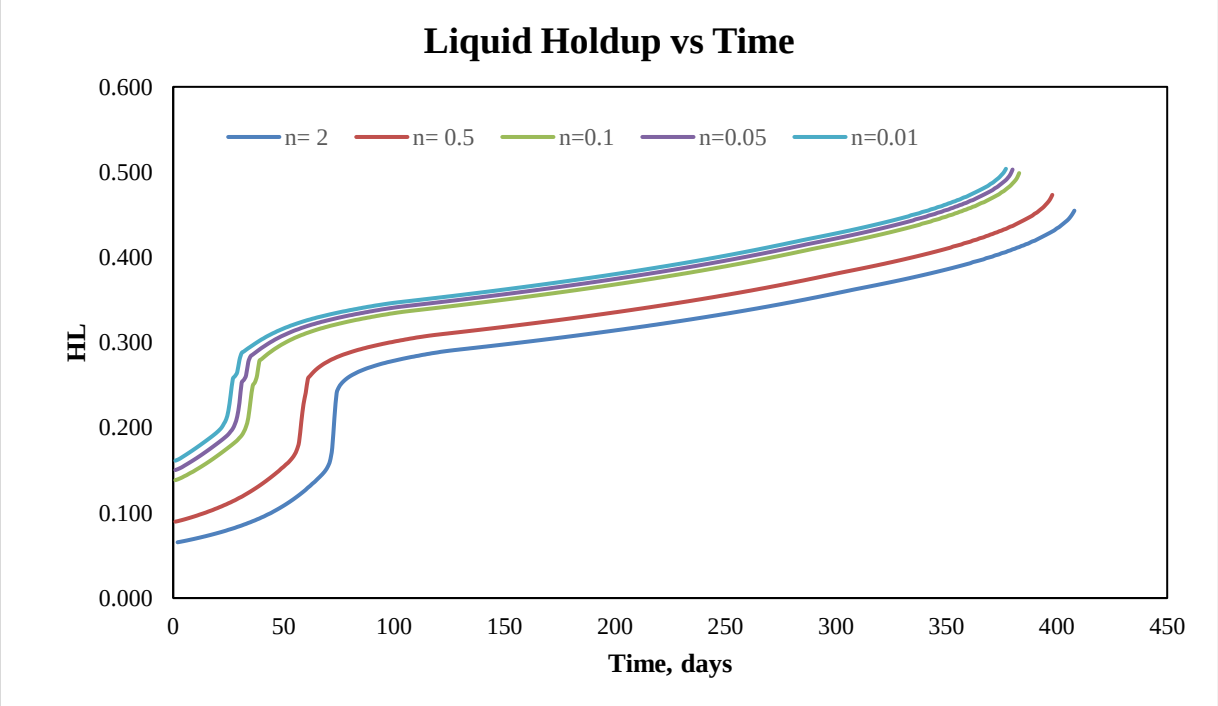

Figure 23 Decreasing Cory exponent below one increase water production significantly

Table 18 Water effect on the onset of liquid loading

n	Gas flow rate at onset	Water flow rate at onset	Time of liquid loading onset
2	1,848	5	73
0.5	1,878	177	59
0.1	1,937	455	36
0.05	1,952	513	31
0.01	1,960	563	27
0.001	1,963	575	26
0.0001	1,961	576	26

Corey exponent is the main factor affecting the relative permeability of both phases in the reservoir. After observing the effect of water production on wells life expectancy, we have increased the water production by lowering the Corey exponent further. The results are summarized in Figure 24 and Table 18. We can see from both that this time the water production is affecting the time of liquid loading onset. When water production becomes in hundreds of barrels, the onset happens faster. However, after decreasing the Corey exponent below a specific value, the liquid onset time does not change because the water production is not changing. The equation itself can explain the reason behind this. When the Corey exponent approaches zero, the value for water relative permeability reaches a constant value.

Depth vs. Liquid Holdup

One of the main conclusion stated in Riza (2016) work is the requirement of studying the onset of liquid loading in the entire wellbore. Previous studies concentrated on the conditions at the wellhead. In this section, we are going to plot the liquid loading vs. the depth and both gas and liquid velocities against depth trying to determine the location at which the liquid loading occurs.

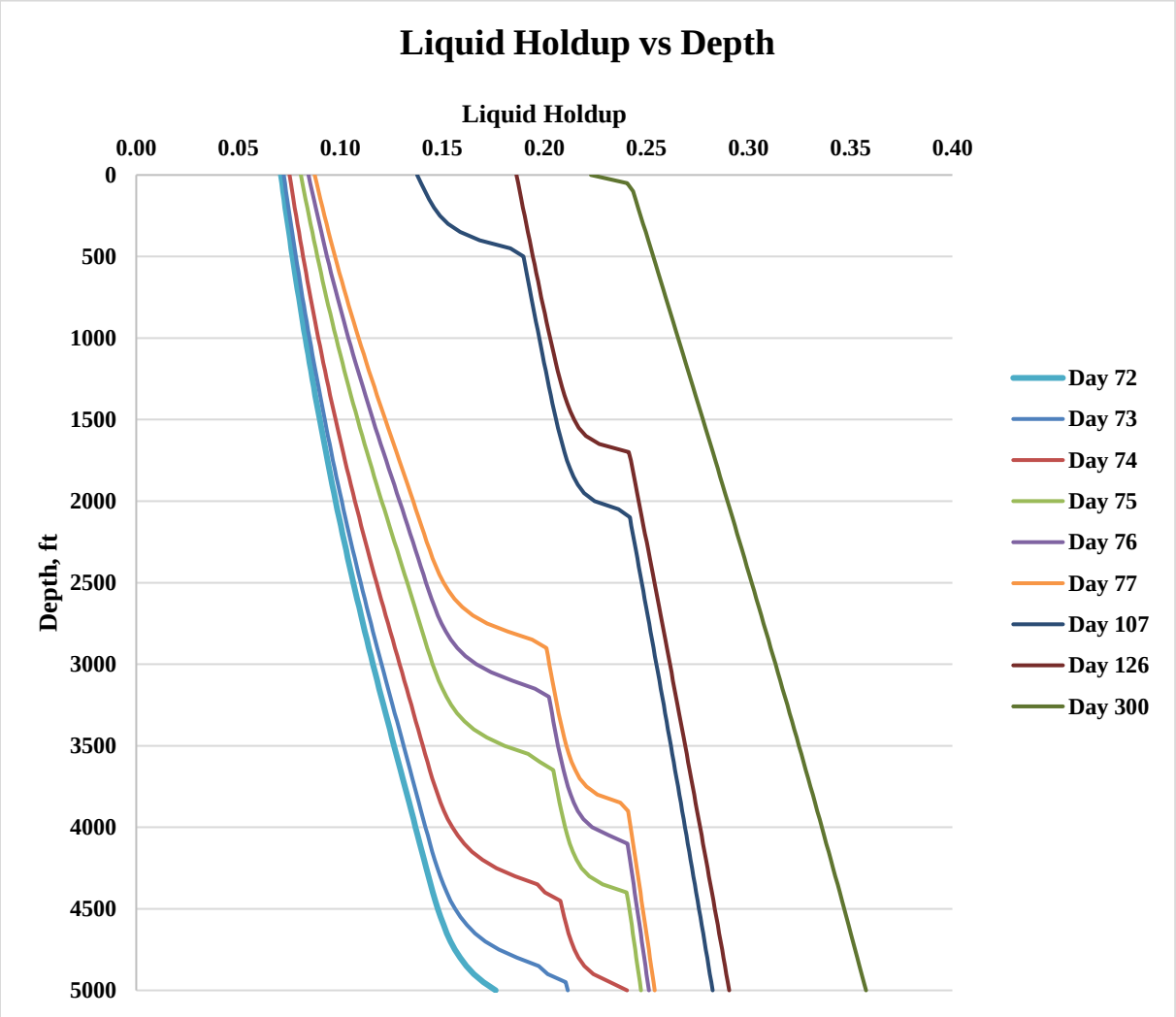

Figure 24 Liquid loading behavior with depth recorded for different days for the same well.

Liquid holdup which is the volume of liquid occupying a segment in the pipe over the volume of that segment is changing throughout the entire wellbore. Even if the volume of liquid entering the wellbore is constant, liquid holdup still varies which is the result of slippage velocity and pressure drop in the wellbore due to friction and hydrostatic pressure. The slippage velocity is the difference between the liquid and gas velocity. The liquid is denser than the gas phase. As a result, it is slower. In addition to this, gas velocity decreases as gas moving upward because of friction loss. The higher the gas velocity, the higher would be the pressure loss. As gas velocity decreases flowing from the bottom to the top of the wellbore, the percentages of liquid and gas occupying the segments of the wellbore are changing as a result. In Figure 25, we can see that the liquid loading is increasing as we go down the wellbore.

At the bottom of the wellbore, the pressure is higher than anywhere else in the wellbore which makes gas molecules compressed the most at the bottom of the well. Because of this compression, gas molecules cannot move as fast as the gas flowing in the upper segments of the wellbore making gas velocity the lowest at the bottom of the well. If the gas and liquid velocity are slower, the amount of the liquid in that segment is higher, making liquid holdup values high at the bottom. As pressure is less in the upper segment due to the friction and hydrostatic loss, gas can flow faster pushing the liquid downward making the liquid content in the upper segments less. Hence, the value of liquid content is less.

The shapes of the curve in Figure 25 differ from each other. If we observe the first curve on day 72, we can see a smooth curve belongs to one mathematical function. However, the 73-day curve changes its sloe near the end. This behavior becomes clearer the next day where we see the distinct slops or three different functions. The shape of the curve depends on the flow pattern in that depth. At day 72 the flow pattern is linear from top to bottom. In day 74, it starts

with an annular flow, then switches to churn flow at a depth of 4,400 ft, the quickly changes into slug flow at 4,470 ft. This behavior continued for the following days. We notice that the annular flow curve is becoming shorter with time oppose to churn and slug flow which dominates the curve with time. One more thing is worth mentioning is that the churn flow at later days when it reaches the top segment of the well it started to decrease again, and the well is dominated only with slug flow.

Gas and Liquid Superficial Velocities Profiles with Depth

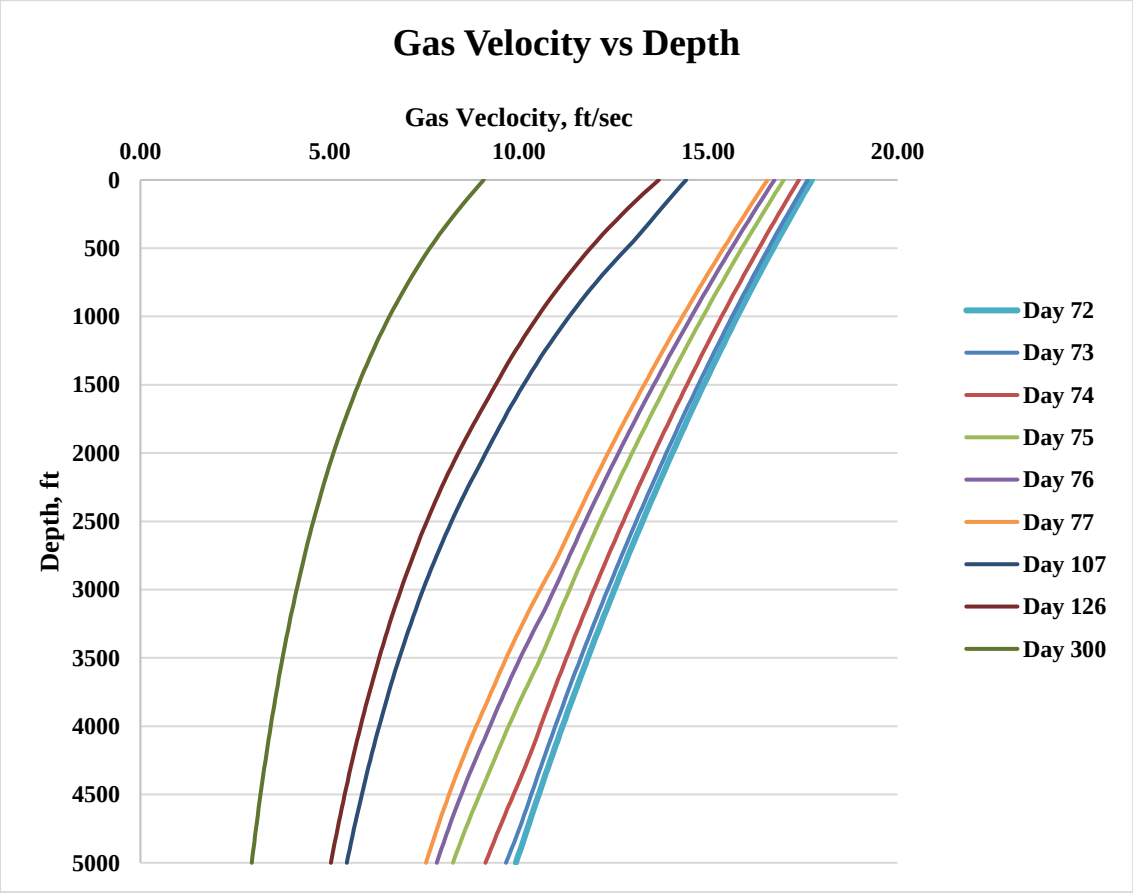

Figure 25 Gas velocity profile versus depth at different days of production

Figure 26 displays superficial gas velocity versus depth for the same well at different well-life stages. In general, gas velocity decreases with time as reservoir pressure is decreased which explains the reduction of gas velocity every day in production. If we look at the well only for one day, the gas velocity decreases as depth increases which is due to the nature of the gas phase as the gas molecules are compressed at the high pressure reducing its velocity. Another interesting finding is that the shape of the curve for each day. The slop for each curve increases as it gets later in well-production which can be related to the flow pattern inside the wellbore at these days. In the beginning, annular flow is the dominated flow pattern. At later stages, slug flow is the most dominated flow pattern. In other words, gas velocity decreases more in a slug dominated flow pattern.

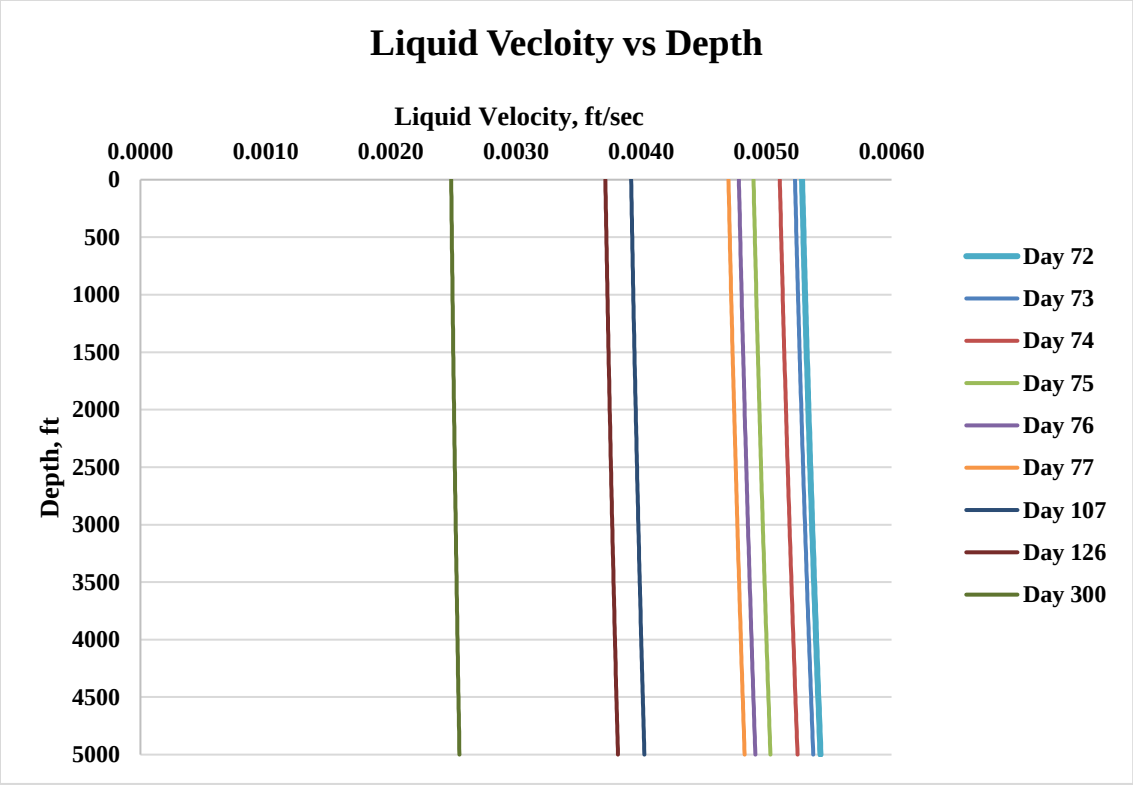

Figure 26 Liquid velocity profile versus depth for one gas well at different days of production

The velocity profile in Figure 27 shows that liquid velocity stays the same throughout the entire wellbore which is due to the nature of the liquid phase. The liquid is incompressible or slightly compressible not like the gas phase. The liquid molecules do no compress under different pressure values. As a result, their velocity stays the same. Liquid velocity decreases with time as reservoir pressure depletes which is the same as gas velocity.

Total, Hydrostatic, and Friction Pressure Drop in Wellbore

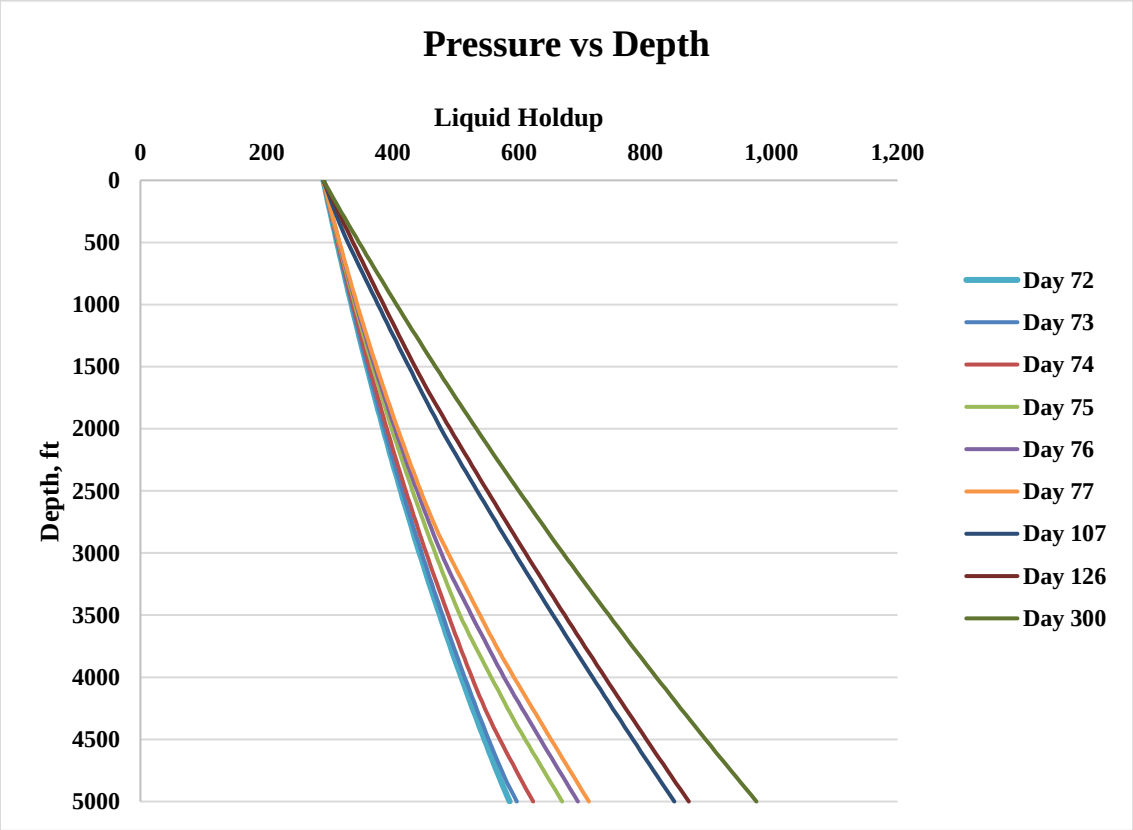

Figure 27 Pressure profile inside the wellbore versus depth

The pressure inside the wellbore decreases as we go from bottom to surface (Figure 28). Pressure loss is due to friction and hydrostatic pressure drop. We observe that at day 300, the pressure drop is the biggest. Pressure drop can be measured as the difference between the buttonhole pressure and wellhead pressure. At earlier days the dominated flow pattern is annular

flow during which liquid content is less than slug flow. Hence, pressure drop due to hydrostatic pressure is less.

In two phase-flow, pressure drop one of the main issues. There are three components of the pressure drop system that cause a pressure drop in the wellbore.

Pressure drop = hydrostatic pressure + friction pressure + kinetic pressure

Kinetic pressure drop is usually ignored as it occurs where there is a change in the wellbore diameter. The weight of the matter causes the hydrostatic pressure drop. In the wellbore, it is a function of density. Since the liquid is the denser phase, this term is mainly associated with the liquid phase. The contribution of gas is insignificant. Friction factor, on the other hand, is mainly linked to the velocity of both phases. It represents the molecules of the matter hitting the tubing wall causing heat, pressure drop. In this section, we will present the pressure drop components for one well over different days of production.

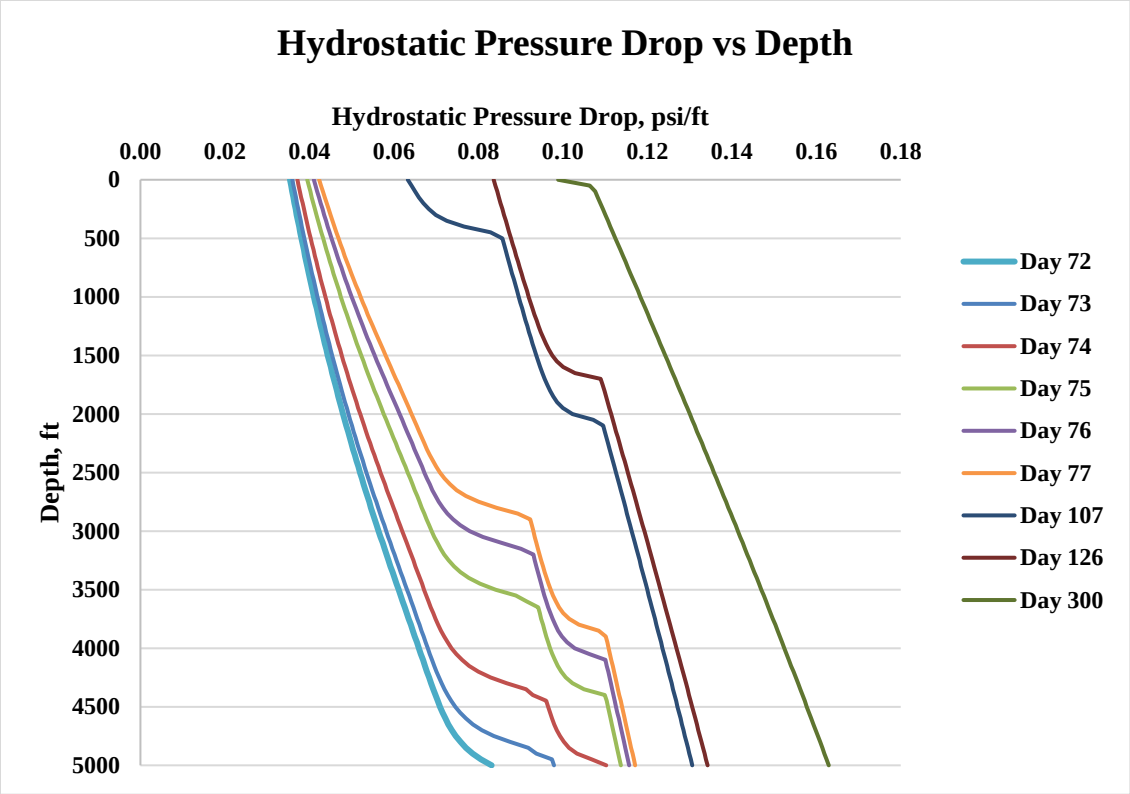

Figure 28 Hydrostatic pressure drop profile at different days of production

Pressure drop due to the weight of the fluid inside the wellbore shown in Figure 29 is almost identical to the liquid holdup profile in Figure 25. The only difference is a constant shift that can be explained from the original equations used to calculate hydrostatic pressure drop and liquid holdup. Let's recall Eq.17 and Eq.40

$$\rho_m = f_g \rho_g + f_l \rho_l \qquad 17$$

$$\frac{\Delta p_h}{L} = \frac{\rho_m}{144} \sin \alpha \qquad 40$$

Hydrostatic pressure drop is a function of fluid mixture density which depends mainly on liquid holdup which is a supporting evidence that hydrostatic pressure drop is linked directly to the liquid content in the wellbore. We can draw the following conclusion; hydrostatic pressure drop is directly proportional to the liquid holdup.

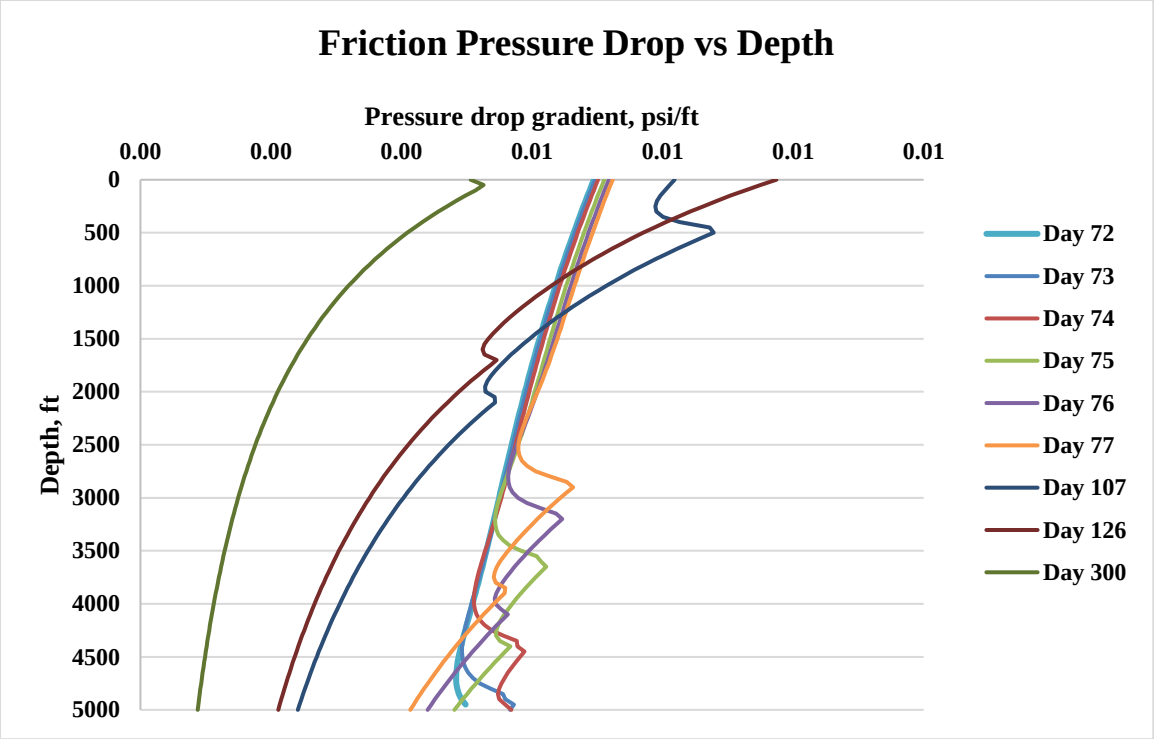

Figure 29 Friction drop gradient profile versus depth at different production days

Friction drop as stated earlier is mainly linked to the velocity of the fluid. Since gas velocity is more significant than liquid velocity, gas is the major contributor to pressure drop due to friction. We expect that the behavior, the gradient, would be different for each flow pattern. Figure 30 shows the different behaviors in each flow pattern. When one flow pattern is the dominated pattern as in day 72, annular flow domination, and day 300 dominated by slug flow. Both curves have almost one shape curve because the values are generated from one equation. For the other curves, each has three shapes representing the three flow patterns. It is evident that slug flow has the least friction pressure drop due to the poor gas contented compared to other flow patterns. Churn flow has the highest friction pressure drop as the liquid content increases, and gas velocity is relatively high, the flow becomes turbulent. Turbulent flow with a mixture of gas and liquid increases the friction between the fluid and tubing wall.

Applying Arps Decline Equation to Determine Liquid Loading Onset

Arps equation (1948) were developed empirically, but at later years, the scientific ground for them was found and proved. Arps presented three equations, hyperbolic, harmonic, and exponential. All these equations are used to forecast well-production.

Examining the production flow rate over time for a single in Figure 15, we notice that all liquid loading onset happened at the same critical flow rate because of the characteristics of the reservoir itself. If we fixed wellhead pressure at a specific value, for the same mixture coming from the reservoir, the pressure drop in the wellbore would be the same! In other words, at a specific pressure value, the properties of the same mixture are the same. It does not matter whether the starting pressure is high or low. Based on this finding, we are going to implement the Arps exponential equation to predict the onset of liquid loading. The equation for exponential decline curve is

$$q_c = q_i e^{-Dt} \tag{55}$$

The critical flow rate which is the flow rate at which the gas flow is unable to carry the liquid droplet to the surface is a function of initial flow rate, time, and the decline coefficient. This equation can be utilized in different ways. One of which is to run the model for one time only to get the critical flow rate for a specific well. Then apply the equation for the prediction of future onset of liquid loading. Rearranging Eq. 55 to calculate the onset of the liquid loading:

$$t_{onset} = \frac{\ln\left(\frac{q_i}{q_{at\,onset}}\right)}{D} \tag{56}$$

Conclusion

Creating coupled wellbore-reservoir two-phase fluid flow model based on simple implicit concepts has proven to be useful. The outcomes of this study will be presented in a bullet points format.

We were able to build a coupled wellbore-reservoir model in a way that has not been done before by combing three main components in an implicit approach. mechanistic pressure drop and heat transfer in the wellbore is the first component. Reservoir inflow equations for both the gas and the liquid phases and the relative permeability equations are the second component. The last component is material balance and in place hydrocarbon volumetric equation.

The model can be run with only a few input data. Reservoir basic properties, basic wellbore data, initial reservoir pressure, and the wellhead pressure.

The model surpassed the oversimplified coupled models presented in the literature by calculating bottomhole pressure and the reservoir pressure at the same time. This implicit approach allows the calculation for both phases flow rates.

The ability to calculate the liquid flow rate in a gas reservoir model is due to the utilizing of relative permeability curves. The implementation of relative permeability curve in production engineering to study the wellbore flow is rarely done.

The proposed model has been validated against three types of validation, commercial software, field data, and open source numerical simulation.

Reservoir pressure has proved to affect liquid loading phenomena directly. It is the biggest impact.

Reservoir initial pressure plays a vital role in deciding how flow pattern changes in the wellbore. The higher the initial reservoir pressure, the longer the wellbore is expected to be in the

annular two-phase flow. However, the longer the well stays in annular two-phase flow, the more likely the flow pattern would change directly from annular two-phase flow into slug flow.

Churn flow is considered the transition phase between annular two-phase flow and slug flow. The stream loses less pressure due to friction and hydrostatic when it is in churn flow. In other words, staying in churn flow for some time after the onset of liquid loading can help in extending the well life expectancy.

The higher the initial reservoir pressure, it would defiantly delay the onset of liquid loading but at the same time reducing the time for the transition from annular two-phase to slug flow. When in slug flow, the stream loses much more pressure in the wellbore and dies faster compared to another well with less initial reservoir pressure.

The proposed model in this study is designed to be a tool for anyone interested in two-phase flow in the wellbore. We have proved this by modifying Hasan-Kabir two-phase flow pressure drop model. The proposed model records the dynamic changes in the wellbore which allowed us to study Hasan-Kabir under various conditions.

We have concluded that Hasan-Kabir model was designed initially for oil phase flow with increasing gas flow. In other word, the gas void fraction starts at a low value and increases as flow pattern changes from bubbly flow up to annular flow which has been observed from the gaps in the liquid holdup curves against depth. The discontinuity in the curves is the result of the smoothing parameters introduced in the original work of Hasan-Kabir model.

We have introduced modified H-K smoothing petameters to be used in gas wells.

Another observation came from the annular flow curve based on H-K model. the curve at lower gas flow rate, when the flow pattern is near changing into churn flow, the curve becomes constant.

H-K model annular two-phase flow equation is an exponential function that reaches a constant value when it reaches the specified limit. Without the addition of a term representing the bubble-rise velocity, the result would be a constant curve before jumping into churn or slug flow creating a discontinuity. To solve this issue, a new term is suggested to be added to the original H-K model to have smooth transitions between all flow patterns.

Liquid holdup onset occurs first at the bottom of the wellbore before anywhere else. The gas velocity at the bottom of the well is the lowest as bottomhole pressure is the highest pressure in the wellbore system. Gas molecules under higher pressure move at a slower pace at which, the gas stream cannot lift all the liquid to the surface which explains the higher liquid holdup values at the bottomhole.

The proposed model gives more than 35 outputs data. Among the output data pressure loss due to friction and hydrostatic pressure. We have observed that pressure drop due to fiction is not the highest in annular two-phase flow as one might expect since gas is the dominated phase and the gas is flowing at high velocity. In churn flow, the pressure drop due to friction is the highest. At churn flow, the velocity is relatively high, and the liquid content has increased which creates turbulent flow. The characteristics of turbulent flow explain the high friction in the churn flow pattern.

The proposed model opens the door to investigate different wellbore pressure drop models. Also, the ability to examine different settings such as inclined wells, horizontal wells, transient inflow, and so much more.

From our observation of annular two-phase flow production curve vs. time, we noticed the behavior is like the exponential decline curve equation known as Arps decline equations. Utilizing this equation can aid in predicting the onset of the liquid loading.

REFERENCES

Alamu, M. B. 2012. Gas-Well Liquid Loading Probed with Advanced Instrumentation. SPE J. 17 (1): 251-270. SPE-153724-PA.

Arps, J. J.: "Analysis of Decline Curves" Trans., AIME (1945) 160,228-247.

A. Zapke and D.G. Kroger. Countercurrent gas-liquid flow in inclined and vertical ducts II: Flow patterns, pressure drop characteristics and ooding. Int. J. Multiphase Flow, 26(2000):1439-1455.

Belfroid, Stefan, Wouter Schiferli, Garrelt Alberts et al. 2008. Prediction Onset and Dynamic Behaviour of Liquid Loading Gas Wells. Proc., SPE Annual Technical Conference and Exhibition, Denver, Colorado, USA.

Brooks, R. H., and Corey, A. T. 1966. Properties of Porous Media Affecting Fluid Flow. J. Irrig. Drain E-ASCE 92 (2): 61-90.

Craft, B. C. and Hawkins, M. F., Applied Petroleum Reservoir Engineering, Prentice-Hall, Inc., Englewood Cliffs, New Jersey, (1959) 39-43

Hasan, A.R. 1995. Void Fraction in Bubbly and Slug Flow in Downward Two-Phase Flow in Vertical and Inclined Wellbores. SPE Production & Operations 10 (3): pp. 172-176.

Hasan, A.R, and Kabir, C.S,. 2002. Fluid Flow and Heat Transfer in Wellbores. Society of Petroleum Engineers Press. Print. Houston, USA.

Hewitt, G. F. 2012. Churn and Wispy Annular Flow Regimes in Vertical Gas–Liquid Flows. Energy & Fuels 26 (7): 4067-4077.

Limpasurat, A., Valko, P. P., Falcone, G. 2015. A New Concept of Wellbore-Boundary Condition for Modeling Liquid Loading in Gas Wells. SPE J. 20 (3): 550 - 564. SPE-166199-PA.

Luo, S., Kelkar, M., Pereyra, E. et al. 2014. A New Comprehensive Model for Predicting Liquid Loading in Gas Wells. SPE Prod & Oper 29 (4): 337-349. SPE-172501- PA.

Li, M., Li, S. L., & Sun, L. T. 2002. New View on Continuous-Removal Liquids from Gas Wells. Society of Petroleum Engineers.

Mulyadi, H., Amin, R., & Kennaird, A. F. 2001. Practical Approach to Determine Residual Gas Saturation and Gas-Water Relative Permeability. Society of Petroleum Engineers.

OL Pushkina and Yu L Sorokin. Breakdown of liquid film motion in vertical tubes. Heat Transfer Sov. Res, 1(5):56–64, 1969.

Riza, M. F., Hasan, A. R., & Kabir, C. S. 2016. A Pragmatic Approach to Understanding Liquid Loading in Gas Wells. Society of Petroleum Engineers.

Sutton, Robert P., S.A. Cox, James F. Lea et al. 2010. Guidelines for the Proper Application of Critical Velocity Calculations. SPE Production & Operations 25 (2): pp. 182-194.

Taitel, Y., Barnea, D. and A.E. Dukler. 1980. Modeling Flow Pattern Transition for Steady Upward Gas-Liquid Flow in Vertical Tubes. Journal of AIChE 33 (2): pp. 345-354.

Turner, R.G., M.G. Hubbard, A.E. Dukler. 1969. Analysis and Prediction of Minimum Flow Rate for the Continuous Removal of Liquids from Gas Wells. Journal of Petroleum Technology 246 (8): pp. 1475-1482.

Waltrich, P.J., Falcone, G., Barbosa Jr., J.R. (2011). Performance of Vertical Transient Two-Phase Flow Models Applied to Liquid Loading in Gas Wells. Paper SPE 147128 presented at the SPE Annual Technical Conference and Exhibition. Denver, CO, USA. 30 October – 2 November.

Wang, X. 2010. Experimental and Numerical Studies on Multiple Well Pairs Sagd Performance, University of Alberta.

van't Westende, J.M.C., H.K. Kemp, R.J. Belt, L.M. Portela, R.F. Mudde, R.V.A. Oliemans. 2008. On the role of droplets in cocurrent annular and churn-annular pipe flow Journal of Heat Transfer and Multiphase Flow 33(9): pp. 595-615.

Veeken, Kees, Bin Hu, Wouter Schiferli. 2010. Gas-Well Liquid-Loading-Field-Data Analysis and Multiphase-Flow Modeling. SPE Production & Operations 25 (3): pp. 275-284.

Veeken, C. A. M., & Belfroid, S. P. C. 2011. New Perspective on Gas-Well Liquid Loading and Unloading. Society of Petroleum Engineers

Zhou, Desheng, Hong Yuan. 2010. A New Model for Predicting Gas-Well Liquid Loading. SPE Production & Operations 25 (2): pp. 172-181.

APPENDIX A

NOMENCLATURE

$p_{wf,wh}$	Bottomhole pressure calculated backward from the wellhead, psi
$p_{wf,\mathrm{Re}}$	Bottomhole pressure calculated from reservoir inflow equation, psi
p_{wf}	Bottomhole pressure, psi
f	Friction factor
z	Gas compressibility factor
ρ_g	Gas density, lbm/ cu ft
k_g	Gas effective permeability, md
q_g	Gas flow rate, SCF/d
B_g	Gas formation volume factor, cu ft/SCF
k_{rg}	Gas relative permeability, md
B_{gi}	Gas reservoir initial formation volume factor, cu ft/SCF
v_{sg}	Gas superficial velocity, ft/s
μ_g	Gas viscosity, cp
$\sigma_{w(280)}$	Gas water interfacial tension at 280 ^{o}F, dynes/cm
$\sigma_{w(74)}$	Gas water interfacial tension at 74 ^{o}F, dynes/cm
$\sigma_{w(T)}$	Gas water interfacial tension at any temperature, dynes/cm

G_i	Initial gas in place, SCF
s_{wi}	Initial water saturation
ρ_l	Liquid density, lbm/ cu ft
f_l	Liquid holdup
v_{sl}	Liquid superficial velocity, ft/s
μ_l	Liquid viscosity, cp
ρ_m	Mixture density, lbm/ cu ft
v_m	Mixture velocity, ft/s
μ_m	Mixture viscosity, cp
M_w	Molecular weight, lb mole-lbm
dp	Pressure drop, psi
$\frac{dp}{dl}_f$	Pressure gradient due to friction, psi/ft
$\frac{dp}{dl}_h$	Pressure gradient due to hydrostatic, psi/ft
P	Pressure, psi
G_p	Produced gas, SCF
z_i	Reservoir initial gas compressibility factor
p_i	Reservoir initial pressure, psi
ϕ	Reservoir porosity, a fraction
r_e	Reservoir radius, ft

A	Reservoir thickness, ft
h	Reservoir thickness, ft
s_w	Reservoir water saturation
s_{gr}	Residual gas saturation
s_{wr}	Residual water saturation
k	Rock absolute permeability, md
T	Temperature, ^oF
a	Tubing area, ft^2
d	Tubing diameter, in
f_g	Void fraction
k_w	Water effective permeability, md
q_w	Water flow rate, STB/d
B_w	Water formation volume factor, bbl/STB
k_{rw}	Water relative permeability, md
μ_w	Water viscosity, cp
θ	Wellbore deviation angle, degree
r_w	Wellbore radius, ft
L	Wellbore segment, ft

APPENDIX B

GAS COMPRESSIBILITY CALCULATION PROCEDURES

$$Z = 0.27\frac{P_r}{T_r\rho}$$

$$f(\rho) = a\rho^6 + b\rho^3 + c\rho^2 + d\rho + e\rho^3\left(1 + f\rho^2\right)\exp\left(-f\rho^2\right) - g = 0$$

$a = 0.06423$

$b = 0.5353Tr-0.6123$

$$c = 0.3151T_r - 1.0467 - \frac{0.5783}{T_r^2}$$

$d = T_r$

$$e = \frac{0.6816}{T_r^2}$$

$f = 0.6845$

$g = 0.27P_r$

$$df(\rho) = 6a\rho^5 + 3b\rho^2 + 2c\rho + d + e\rho^2\left(3 + f\rho^2\left(3 - 2f\rho^2\right)\right)\exp\left(-f\rho^2\right)$$

$$\rho_{new} = \rho_{old} - \frac{f(\rho)}{df(\rho)}$$

$$\frac{\partial Z}{\partial T} = 0.27P_r\left[\frac{\partial(1/T_r)}{\rho\partial T} + \frac{1}{T_r}\frac{\partial(1/\rho)}{\partial T}\right] = 0.27P_r\left[\frac{1}{T_cT_r^2\rho} - \frac{1}{T_r\rho^2}\frac{\partial\rho}{\partial T}\right] = 0.27\frac{P_r}{T_r\rho}\left[\frac{1}{T} + \frac{1}{\rho}\frac{\partial\rho}{\partial T}\right]$$

$$\frac{df(\rho)}{dT} = \left[6a\rho^5 + 3b\rho^2 + 2c\rho + d + e\rho^2\left(3 + f\rho^2\left(3 - 2f\rho^2\right)\right)\exp\left(-f\rho^2\right)\right]\frac{d\rho}{dT}$$
$$+ \frac{1}{T_c}\left[b_1\rho^3 + c_1\rho^2 + 2c_3\frac{\rho^2}{T_r^3} + \rho - 2e_1\frac{\rho^3}{T_r^3}\left(1 + f_1\rho^2\right)\exp\left(-f\rho^2\right)\right] = 0$$

Rewriting it as $A\frac{d(\rho)}{dT} + B = 0$ we obtain $\frac{d\rho}{dT} = \frac{A}{B}$

$$A = \left[6a\rho^5 + 3b\rho^2 + 2c\rho + d + e\rho^2\left(3 + f\rho^2\left(3 - 2f\rho^2\right)\right)\exp\left(-f\rho^2\right)\right] = df(\rho)$$

$$B = \frac{1}{T_c}\left[b_1\rho^3 + c_1\rho^2 + 2c_3\frac{\rho^2}{T_r^3} + \rho - 2e_1\frac{\rho^3}{T_r^3}\left(1 + f_1\rho^2\right)\exp\left(-f\rho^2\right)\right]$$

Reservoir gas compressibility factor is calculated implicitly

$$xy = 0.27\frac{p_r}{T_r z}$$

$$f_{xy} = 0.06423\,xy^6 + \left(0.5353T_r - 0.6123\right)xy^3 + \left(0.3151T_r - 1.0467 - \frac{0.5783}{T_r^2}\right)xy^2 + T_r + \frac{0.6816}{T_r^2}xy^3\left(1 + 0.6845\,xy^2\right)e^{\left(-0.6845xy^2\right) - 0.27p_r}$$

APPENDIX C

PROPOSED MODEL CODE EXPLAINED

Modeling Summary Flow Chart

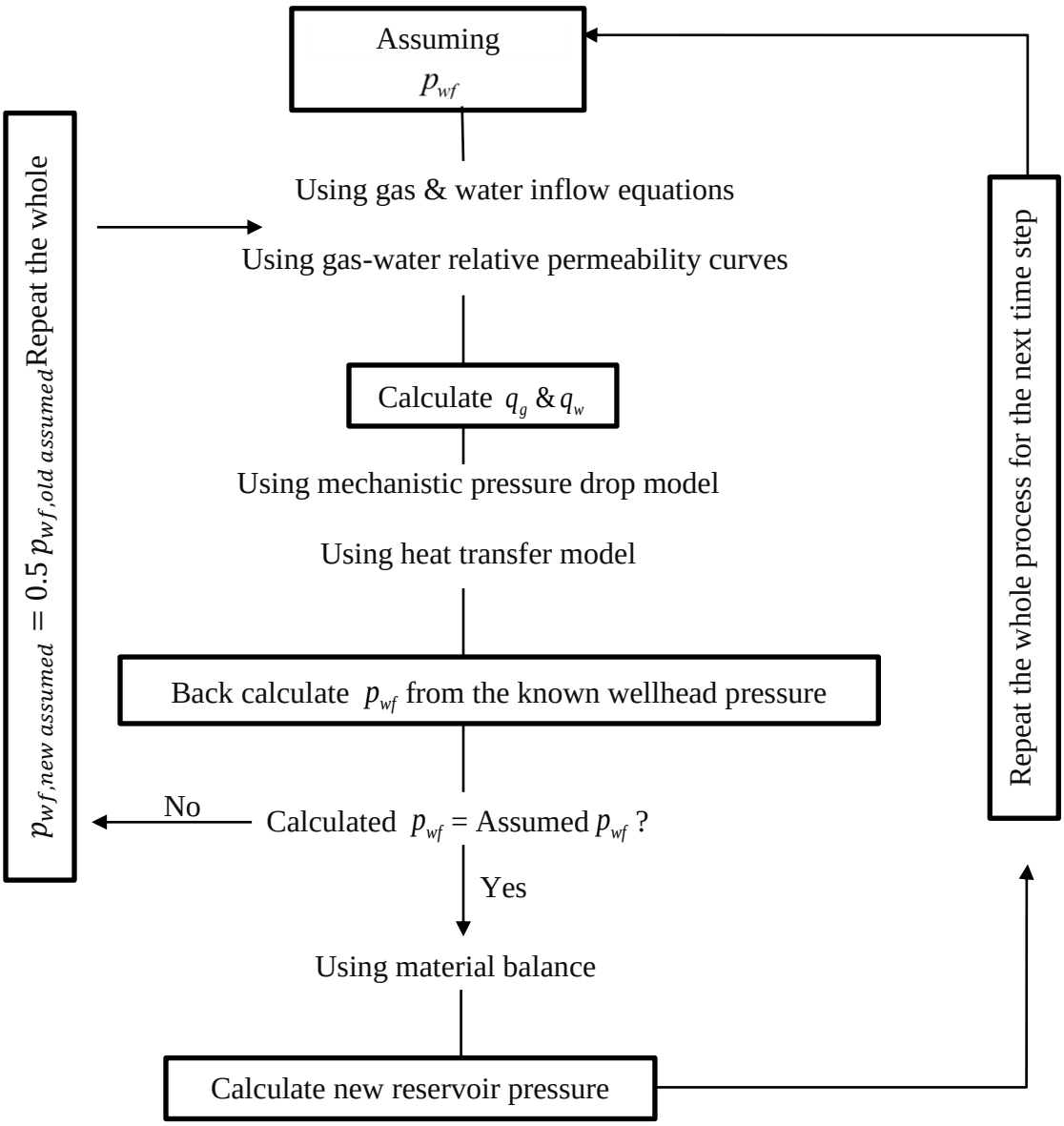

```
\\\\\\ Declaring the constants
    Pi = 4 * Atn(1)
    g = 32.2
    gc = 32.2
    R = 10.732
 ' Time
    tt = Sheet2.Cells(2, 5)     \\\\\ Time steps specified by the user
    Period = Sheet2.Cells(2, 8)  \\\\ Simulation Time
\\\\\Reservoir Input Data
   Pri = Sheet2.Cells(4, 3)
    TR = Sheet2.Cells(5, 3)
    RA = Sheet2.Cells(6, 3)
    k = Sheet2.Cells(7, 3)
    h = Sheet2.Cells(8, 3)
    porosity = Sheet2.Cells(9, 3)
    swi = Sheet2.Cells(10, 3)
    swr = 0.17
    sgr = (1 - swr) * 0.1813 + 0.096071
    den_L = Sheet2.Cells(11, 3)
    re = (RA * 43560 / Pi) ^ 0.5
\\\\ Stream Input data
    Tpc = Sheet2.Cells(17, 3)     \\\\\Pseudo Critical T
    Ppc = Sheet2.Cells(18, 3)     \\\\\Pseudo Critical P
```

```
    MW = Sheet2.Cells(19, 3)       \\\\\Gas Molecular Weight
    sg = Sheet2.Cells(20, 3)       \\\\\Gas specific gravity
   \\\\\\\ Original gas in place
    zi = z_factor(Pri, TR, Ppc, Tpc)
     Sheet2.Cells(4, 13) = zi
    pr = Pri
    zr = zi
    sw = swi
    bgi = 0.0283 * (TR + 460) * zi / Pri
    Sheet2.Cells(5, 13) = bgi
    gi = 43560 * RA * h * porosity * (1 - swi) / bgi
    Sheet2.Cells(6, 13) = gi / 1000000
pwf1 = pr - 200
pwf2 = pwf1 + 1
Dim Time As Integer
Time = (tt / Period) - 1
For n = 0 To Time     \\\\\\\ Starting the bigger loop
       pwb = pwf1 + 1
       Do Until Abs(pwf1 - pwb) < 1   \\\\\ The loop for the well 100 segments
  \\\\\\ Wellbore input data
             Pwh = Sheet2.Cells(4, 9)
             twh = Sheet2.Cells(5, 9)
             d = Sheet2.Cells(7, 9) / 12
```

```
        E = Sheet2.Cells(8, 9)        ' Pipe Roughness ft
        a = Pi / 4 * d ^ 2
        Sheet2.Cells(10, 13) = a
        alpha = Sheet2.Cells(9, 9) * Pi / 180
        d_o = Sheet2.Cells(10, 9)
        d_i = Sheet2.Cells(11, 9)
        rw = Sheet2.Cells(12, 9)
        Depth = Sheet2.Cells(13, 9)       ' Well depth
    \\\\\\\ Reservoir In flow calculation
        den_g = pr * MW / zr / R / (TR + 460)
        vis_g = Gas_Viscosity(MW, TR, den_g)
        'krg = (1 - (sw - swr) / (1 - swr - sgr)) ^ 2 * (1 - ((sw - swr) / (1 - swr - sgr)) ^ 2)
        krg = ((1 - sw - sgr) / (1 - sgr)) ^ 2
        kg = krg * k
        qg = (pr ^ 2 - pwf1 ^ 2) * kg * h / 1424 / vis_g / zr / (TR + 460) /
WorksheetFunction.Ln(0.472 * re / rw)
      'qg = (1 - 0.2 * pwf1 / pr - 0.8 * (pwf1 / pr) ^ 2) * qg_max
         'krw = ((sw - swr) / (1 - swr - sgr))
        krw = ((sw - swr) / (1 - swr)) ^ 2
        kw = krw * k
        Bw = water_formation(pr, TR)
        vis_w = Exp(1.003 - 1.479 * 10 ^ -2 * TR + 1.982 * 10 ^ -5 * TR ^ 2)
    qw = kw * h * (pr - pwf1) / 141.2 / Bw / vis_w / WorksheetFunction.Ln(0.472 * re / rw)
```

```
'Wellbore ----------------------------------------------------------------
pwb = Pwh
dp = 0
For i = 0 To 100
Count = Count + 1
twb = twh + i * (TR - twh) / 100
pwb = pwb + dp
segma = 75 - 1.108 * pwb ^ 0.349 + ((twb - 74) * (53 - 0.1048 * pwb ^ 0.637) - (twb -
74) * (75 - 1.108 * pwb ^ 0.349)) / 206
z = z_factor(pwb, twb, Ppc, Tpc)
den_g = pwb * MW / z / R / (twb + 460)
vis_g = Gas_Viscosity(MW, twb, den_g)
vis_l = Exp(1.003 - 1.479 * 10 ^ -2 * twb + 1.982 * 10 ^ -5 * twb ^ 2)
Bg = 0.0283 * (twb + 460) * z / pwb
Bw = water_formation(pwb, twb)
vsg = qg * 1000 * Bg / 24 / 60 / 60 / a
vsl = qw * Bw * 5.615 / 24 / 60 / 60 / a
vm = vsl + vsg
vgc = 3.1 * (g * segma * 0.0022048 * (den_L - den_g) / den_g ^ 2) ^ 0.25
vgb = (0.43 * vsl + 0.36 * 1.53 * (g * (den_L - den_g) * segma * 0.0022048 / den_L ^ 2) ^ 0.25)
* Sin(alpha)
' Flow Patern
If vsg > vgc Then
```

```
fp = "Annular"
co = 1.15 * (1 - Exp(-0.2 * vgc / (vsg - vgc))) + Exp(-0.2 * vgc / (vsg - vgc))
vb = 1 - Exp(-0.01 * vgc / (vsg - vgc))
ElseIf vsg < vgb Then
fp = "Bubbly"
vb = 1.53 * (g * (den_L - den_g) * segma * 0.0022048 / den_L ^ 2) ^ 0.25
co = 1.2
ElseIf vm > (4.68 * d ^ 0.48 * (segma * 0.0022048 / den_L) ^ 0.6 * ((den_L - den_g) * g / segma / 0.0022048) ^ 0.5 * (den_L / vis_l) ^ 0.08) ^ (1 / 1.12) Then
fp = "Churn"
co = 1.15 * Exp(-0.01 * ((4.68 * d ^ 0.48 * (segma * 0.0022048 / den_L) ^ 0.6 * ((den_L - den_g) * g / segma / 0.0022048) ^ 0.5 * (den_L / vis_l) ^ 0.08) ^ (1 / 1.12)) / (vm - ((4.68 * d ^ 0.48 * (segma * 0.0022048 / den_L) ^ 0.6 * ((den_L - den_g) * g / segma / 0.0022048) ^ 0.5 * (den_L / vis_l) ^ 0.08) ^ (1 / 1.12)))) + 1.2 * (1 - Exp(-0.01 * ((4.68 * d ^ 0.48 * (segma * 0.0022048 / den_L) ^ 0.6 * ((den_L - den_g) * g / segma / 0.0022048) ^ 0.5 * (den_L / vis_l) ^ 0.08) ^ (1 / 1.12)) / (vm - ((4.68 * d ^ 0.48 * (segma * 0.0022048 / den_L) ^ 0.6 * ((den_L - den_g) * g / segma / 0.0022048) ^ 0.5 * (den_L / vis_l) ^ 0.08) ^ (1 / 1.12)))))
vb = 0.35 * (g * d * (den_L - den_g) / den_L) ^ 0.5 * (1 + Cos(alpha)) ^ 1.2 * (Sin(alpha)) ^ 0.5
Else
fp = "Slug"
co = 1.2
```

```
                vb = 1.53 * (g * (den_L - den_g) * segma * 0.0022048 / den_L ^ 2) ^ 0.25 * (1 -
Exp(-0.1 * vgb / (vsg - vgb))) + 0.35 * (g * d * (den_L - den_g) / den_L) ^ 0.5 * (1 +
Cos(alpha)) ^ 1.2 * (Sin(alpha)) ^ 0.5 * Exp(-0.1 * vgb / (vsg - vgb))
                End If
            \\\\\\\\\\\\ Pressure Drop Calculation
                fg = vsg / (co * vm + vb)
                fl = 1 - fg
                den_m = fg * den_g + den_L * fl ' den = Density   m= mixture
                x = vsg * den_g / vm / den_m
                vis_m = x * vis_g + (1 - x) * vis_l
                ren = den_m * vm * d / vis_m / 0.000672
                f = 0.001375 * (1 + (20000 * E / d + 10 ^ 6 / ren) ^ (1 / 3))
                dph = den_m / 144 * Sin(alpha)
                dpf = f * vm ^ 2 * den_m / 2 / d / 144 / gc
                dp = (dph + dpf) * Depth / 100
        pr = Pri / zi * (1 - gp / gi) * zr
        zr = z_factor(pr, TR, Ppc, Tpc)
      Bgr = 0.0283 * (TR + 460) * zr / pr
    sw = 1 - (gi - gp) * Bgr / 43560 / RA / h / porosity
  ww = ww + 1
Next
        End Sub
```

```
Function z_factor(P, T, Ppc, Tpc)   \\\\\ Function to calculate z factor
    TR = (T + 460) / Tpc
    prr = P / Ppc
    z = 1
    xy = 0.27 * prr / TR / z
        Do Until Abs(Nxy - xy) < 0.0001
        fxy = 0.06423 * xy ^ 6 + (0.5353 * TR - 0.6123) * xy ^ 3 + (0.3151 * TR - 1.0467 - 0.5783
/ TR ^ 2) * xy ^ 2 + TR * xy + 0.6816 / TR ^ 2 * xy ^ 3 * (1 + 0.6845 * xy ^ 2) * Exp(-0.6845 *
xy ^ 2) - 0.27 * prr
        dfxy = 6 * 0.06423 * xy ^ 5 + 3 * (0.5353 * TR - 0.6123) * xy ^ 2 + 2 * (0.3151 * TR -
1.0467 - 0.5783 / TR ^ 2) * xy + TR + 0.6816 / TR ^ 2 * xy ^ 2 * (3 + 0.6845 * xy ^ 2 * (3 - 2 *
0.6845 * xy ^ 2)) * Exp(-0.6845 * xy ^ 2)
        Nxy = xy - fxy / dfxy
        Store = xy
        xy = Nxy
        Nxy = Store
        Loop
    z_factor = 0.27 * prr / TR / xy
End Function
```

```
Function Gas_Viscosity(MW, T, den_g)
 AA = ((9.379 + 0.01607 * MW) * (T + 460) ^ 1.5) / (209.2 + 19.26 * MW + (T + 460))
    BB = 3.448 + 986.4 / (T + 460) + 0.01009 * MW
    CC = 2.447 - 0.2224 * BB
    Gas_Viscosity = AA * 10 ^ -4 * Exp(BB * (den_g * 0.016018463) ^ CC)
End Function
\\\\\\ Function to calculate water formation volume factor
Function water_formation(P, T)
        A1 = 0.9947 + 5.8 * 10 ^ -6 * T + 1.02 * 10 ^ -6 * T ^ 2
        A2 = -4.228 * 10 ^ -6 + 1.8376 * 10 ^ -8 * T - 6.77 * 10 ^ -11 * T ^ 2
        A3 = 1.3 * 10 ^ -10 - 1.3855 * 10 ^ -12 * T + 4.285 * 10 ^ -15 * T ^ 2
        water_formation = A1 + A2 * P + A3 * P ^ 2
End Function
```